Soil Dynamics and Earthquake Engineering 103 (2017) 123–140

Contents lists available at ScienceDirect

Soil Dynamics and Earthquake Engineering

journal homepage: www.elsevier.com/locate/soildyn

Regional subsidence effects on seismic soil-structure interaction in soft clay

Juan M. Mayoral*, Ernesto Castañon, Jorge Albarran

Coordinacion de Geotecnia, Instituto de Ingeniería, Universidad Nacional Autonoma de Mexico, Mexico city, Mexico

ARTICLE INFO

Keywords:
Soil-structure interaction
Soft clay
Dynamic properties
Consolidation

ABSTRACT

Regional subsidence effects on dynamic soil properties and ground layering deformation are often ignored in practice, when dealing with seismic soil-structure interaction analyses. Nevertheless, these effects can substantially change the frequency content and spectral accelerations in both free field and in the soil-structure system. Pore pressure variations over the project economic life are due to both regional subsidence as well as dissipation of excess pore pressure caused by the structure weight. These variations lead to changes in effective stresses, which in turn, modify the dynamic properties such as shear wave velocity distribution and modulus degradation and damping curves, as well as soil layer thickness and shape. These changes can be substantial in highly compressible very soft clay, such as that found in Mexico City valley. This paper presents a numerical study on the seismic response of a conventional five-story building supported by a compensated box foundation built in soft clay, considering these effects. Three-dimensional finite difference models were developed with the software FLAC^{3D}. Initially, the evolution of effective stresses with pore pressure was established based on in-situ piezometer measurements of an instrumented site, and laboratory data. Then, changes in dynamic properties were taken into account based on the results gathered from series of resonant column tests conducted for several effective consolidation stresses, and a PS suspension logging test. The static behavior of the soil-structure system was assessed. For the cases studied herein, the complex interplay between soil nonlinearities, which lead to fundamental period elongation of the soil deposit, T_p, and the overall tendency of ground consolidation to shorten it, controls the variations in the spectral ordinates depending on how close T_p is of the predominant period of the excitation.

1. Introduction

Seismic performance evaluation of soil-structure systems built on very soft high plasticity clays is a complex problem, especially when expected changes in effective stresses during the economic life of the structure due to dissipation of excess pore pressure caused by the building gravity loads and regional subsidence are very large. These changes in effective stresses lead, in turn, to large settlements. This is particularly important in urban areas located in highly compressible clays, such as Mexico City, where the settlement rate of regional subsidence reaches about 10 cm/year in average, but can go as large as 35 cm/year in some areas. Thus, it is common to have ground settlements ranging from 40 to 90 cm, due to load consolidation, and around several meters due to regional subsidence [1]. These settlements produce changes in both soil profile configuration (i.e. layer thickness and geometry), as well as dynamic properties, such as shear wave velocity distribution with depth and modulus degradation and damping curves. These factors impact the seismic response of the soil-structure system. The effect of dynamic properties changes on the seismic response of sites located in soft clay, has been only marginally studied by other researches [2–5], finding that the variation of shear wave velocities and modulus degradation and damping curves with effective confining stresses can modify significantly the computed response. Nevertheless, the impact of these variations in the seismic performance of soil-structure systems has not been addressed, neither the effect of changes in the soil profile configuration after several meters of sinking. These effects however, can drastically modify both free field, near field and structural response over time. This paper presents a numerical study of the seismic response of a conventional five-story building supported by a partially compensated box foundation built in highly compressible soft clay, considering these effects. Three-dimensional finite difference models were developed with the software FLAC^{3D}. Initially, the evolution of effective stresses with the pore pressure was established based on in-situ piezometer measurements, and laboratory data. Then, variations in dynamic properties were taken into account based on a series of resonant column tests conducted for several mean effective consolidation stresses and a suspension logging test. The static behavior of the soil-structure system was assessed. The free field model response

* Corresponding author.
E-mail address: jmayoralv@iingen.unam.mx (J.M. Mayoral).

http://dx.doi.org/10.1016/j.soildyn.2017.09.014
Received 3 January 2017; Received in revised form 18 September 2017; Accepted 21 September 2017

was calibrated for moderate to strong level of shaking (i.e. return periods of 125 and 250 years, respectively) comparing the fully nonlinear analyses results with equivalent linear analyses carried out with the program SHAKE [6]. Finally, the seismic performance of the soil-structure system was studied to evaluate the impact of the changes on dynamic properties and layering configuration on the seismic response, considering an extreme subduction event associated to a 2475 years return period. Insight was gained regarding the complexity of the interplay of the effective stress history, and static and seismic soil-structure performance during an extreme earthquake.

2. Methodology

As it is well known, field evidence has shown that shear wave velocity increase overtime in highly compressible clays, such as those found in Mexico City, can lead to important changes in the seismic response of a given place during the life time of a particular structure [2–5]. Although ground subsidence effects on soil-structure interaction has been addressed for static loading conditions [7,8], to date, there is still a lack of information regarding how to account for this effect in seismic-soil-structure interaction analyses. This paper presents a numerical approach to address this problem to establish the effect of how the changes in effective confining stress can affect the seismic-soil-structure interaction. The proposed approach is comprised of eighth steps as follows: 1) Initial in-situ stress determination based on field data gathered from piezometers, 2) Evaluation of the consolidation evolution over the economic life of the structure, based also on medium to long term piezometers monitoring. Establishing pore water pressures evolution with time at the studied site is a requirement for obtaining the expected consolidation settlements due to regional subsidence, 3) Determination of the volumetric modulus, m_v, variation with the mean effective stresses, for the clayey formations found at the studied site, conducting one-dimensional consolidation tests, 4) Determination of small shear stiffness variation with mean effective consolidation stresses, using resonant column or bender element tests, and correction for field effects considering in-situ shear wave velocity measurements, 5) Ground settlements calculation for each consolidation time considered, employing the analytical solution provided by Terzaghi´s theory for one dimensional consolidation, $\Delta H = m_v p H$, where m_v is the volumetric modulus, H layer thickness, and ΔH the corresponding layer deformation, 6) Site response analyses for each consolidation time considered, 7) Seismic-soil-structure interaction analyses for each consolidation time considered. Depending on the level of shaking it could be necessary to account for soil nonlinearities, and 8) Evaluation of post-earthquake settlements due to seismic-induced excess pore pressure, when dealing with sensitive or low plasticity clays. This evaluation will be required when soil stiffness degradation during cyclic loading leads to an important amount of pore pressure generation.

3. Case study

A conventional five-story building supported by a compensated box foundation located on the Texcoco Lake area (Fig. 1), was considered in the numerical study. Due to the particular characteristics of Mexico City clay having a high plasticity index, no significant reduction in shear modulus is observed even for shear strains as high as 0.1% [9–12]. Similarly, there is no significant increase in the damping ratio until angular distortions of the order of 0.3% are reached. Thus, the response of clayey soil deposits is nearly elastic even for shear strains as high as 0.3%, which leads to a high potential of amplification of the seismic waves. Indeed, amplification factors up to 5 (between peak ground acceleration, PGA, observed at soft soil with respect to those of rock outcrops) were observed during the 1985, Michoacan earthquake. During this event, the long distance that seismic waves needed to travel from the zone of energy release to the Mexico City area (around 390 km), filtered the high frequency waves, leading to have a long

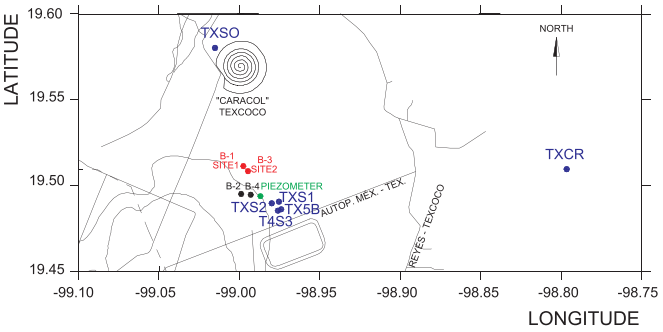

Fig. 1. Seismological stations, exploration borings and piezometer locations.

period ground motion (i.e. the energy is concentrated around 2–3 s). A double resonance effect was caused when the incoming seismic waves reach the city area, due to the fact that both the clayey soils and the most damaged buildings had a fundamental period ranging between 2 to 2.5 s, as well as the earthquake excitation.

3.1. Soil stratigraphy

Soil profiles of Site 1 and Site 2 are presented in Fig. 2. Site 1 presents a desiccated crust of sandy silt at the top extending down to a depth of 1 m, which is underlain by a soft clay layer approximately 28 m thick, with interbedded lenses of volcanic ashes. Underlying this clay, there is a 1 m thick layer of very dense sandy clay and a 3 m thick silt layer. This layer rest on top of a stiff clay layer which goes down to 63 m of depth. Below this layer of clay, there is a second layer of very dense silty sand and sandy silt, often called the second hard layer. Site 2, presents the same layer of desiccated crust of sandy silt at the top, extending down to a depth of 1 m. This stratum is underlain by a soft clay layer approximately 28 m thick, interbedded by lenses of volcanic ashes. Beneath this formation a silt layer 3 m thick is found, followed by series of silty sands lenses down to a depth of 34 m. These layers rest on top of a stiff clay layer which goes down to 62 m, at which the second hard layer is located.

3.2. Piezometric measurements

A piezometer was installed at the instrumented site as depicted in Fig. 1. Initially, the evolution of pore pressure withdrawn with water extraction was established based on the available piezometer readings located at several depths (i.e. 9, 18, 31, 38 and 45 m) as shown in Fig. 3, which presents the evolution of normalized measured pore pressure, u, over the initial reading, u_o. Based on these data, empirically-derived equations were used to estimate the expected evolution of the pore pressure over time. Fig. 4 shows the corresponding computed pore pressure distribution with depth for each time of analysis (i.e. 5, 10, 30 and 60 years). It can be clearly noticed that the initial pore water pressure distribution is not hydrostatic.

3.3. Experimental data

For the subsoil conditions characterization, a total of four exploration borings (B-1, B-2, B-3 and B-4) were conducted (Fig. 1). A combination of cone penetration test, CPT, standard penetration test, SPT, and PS suspension logging, along with a laboratory investigation were conducted to obtain the static and dynamic properties of the soils found at the site for the strains level of interest. The depths of the CPT´s ranged from 50 to 70 m. At those depths where the hardness of the ground exceeded the applicability of this subsoil exploration technique, standard penetration tests, SPT, was used instead. In addition, a 65 m depth SPT was conducted for soil identification purposes, at the same locations. The Shelby sampler was used to obtain undisturbed soil

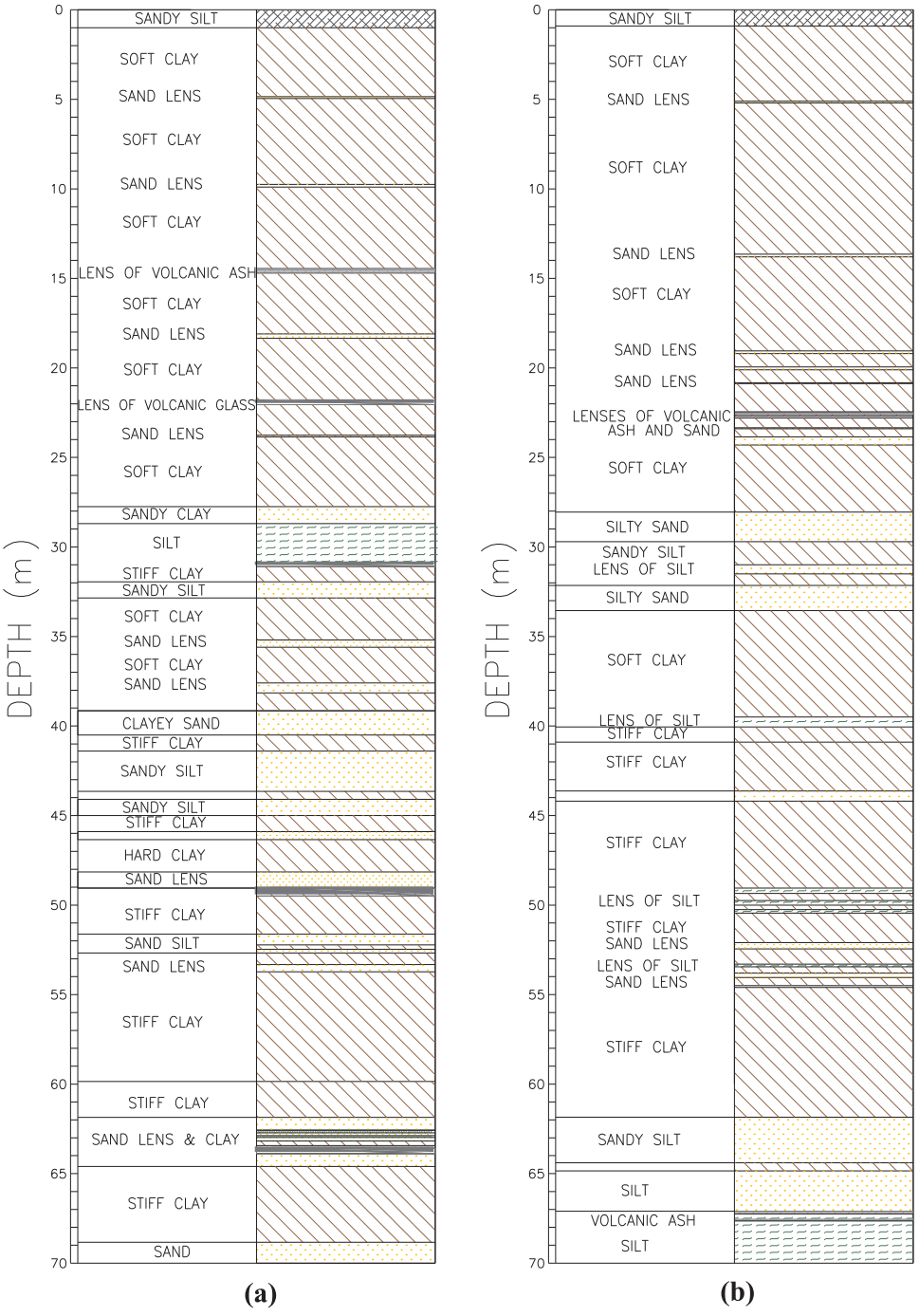

Fig. 2. Soil profiles for (a) Site 1 and (b) Site 2.

samples at the studied zone. The suspension PS logging technique was used in exploration boring B-1 to determine in situ values of shear wave velocity, at the studied Site 1. A total of forty six resonant column and nine cyclic triaxial tests were conducted, for several mean effective consolidation stresses, σ'_c, in nine samples retrieved at the site, and fifty one unidimensional consolidation trials were carried out with incremental load in saturated samples, for several mean effective consolidation stresses. Table 1 summarizes the index properties of the tested soils, including the distribution of water content, w(%), plasticity index, PI, and reference strain, γ_m, for each tested sample. As shown in this table, samples retrieved above 16 m of depth present a high natural water content, varying between 100% and 250%, the plasticity index fluctuates from 150% to 210%. Between 16 and 30 m, w(%) varies from 250% to 300%, and PI values goes from 190% to 210%. For greater depths, a notorious reduction of the plasticity index can be observed (PI < 100%). The volume compressibility parameter, m_v, of the "virgin" and "recompression" branch vary depending on the increase of the mean effective consolidation stresses applied, as shown in Fig. 5, which also includes a numerical regression equation obtained to calculate the parameter m_v for the normally consolidated (i.e. virgin branch) and over consolidated (i.e. recompression branch) soil stages, in both the upper and lower clayey formations. For the deep stiffer silty clay and sandy silt deposits, the parameter m_v was considered constant with the mean effective consolidation stresses.

3.4. Shear wave velocity distribution

The evolution of the shear wave velocity during the time of analysis

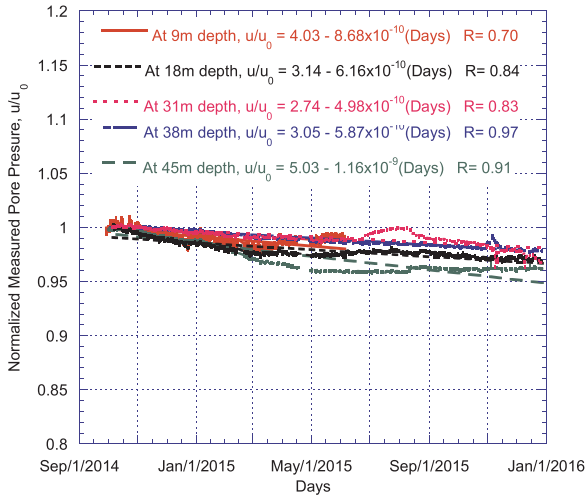

Fig. 3. Pore pressure distribution with depth.

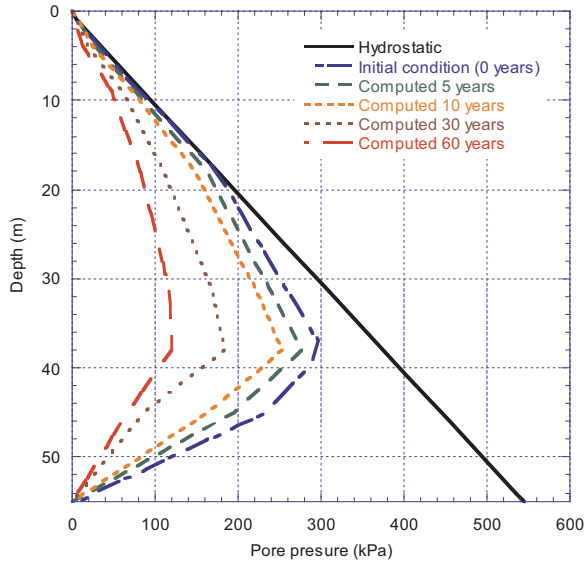

Fig. 4. Evolution of pore pressure distribution.

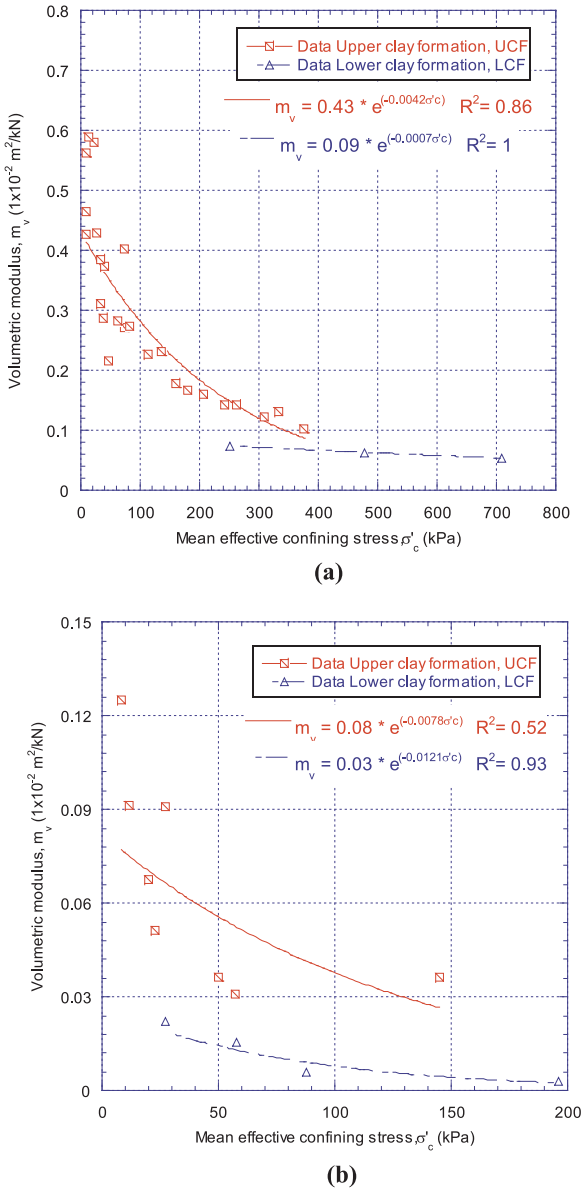

Fig. 5. Variation of the coefficient m_v, in the studied site for (a) "virgin" and (b) "re-compression" soil stages.

was estimated as follows. Initially the variation of shear wave velocity with the mean effective stress was established in the laboratory based on the results obtained from series of resonant column tests as depicted in Fig. 6, which shows the evolution of shear wave velocity with mean effective consolidation stress for several plasticity indexes. A similar approach was followed by [13], but using also the results obtained from bender elements. As pointed out by [11] and [13], the maximum difference observed in the shear wave velocities obtained from various procedures such as resonant column or bender element tests, or even direct field measurements, falls within the 7–15% range. Thus, for the work presented herein, it was deemed appropriate to correct the

Table 1
Index properties of the extracted samples.

Borehole	Sample Number	Depth		w_L	w_P	PI	LI	G_s	w	e	G_w	γ_m
		Initial [m]	Final [m]	[%]	[%]	[%]			[%]		[%]	[kg/m^3]
B-1	1	4.40	5.30	287.4	131.1	156.3	0.78	2.58	253.0	6.68	97.6	1184
	2	15.40	16.30	284.2	72.4	211.8	0.81	3.03	244.9	7.42	100.0	1250
	3	39.50	40.40	181.8	48.4	133.4	0.63	2.71	132.3	3.52	100.0	1405
B-2	4	4.00	4.90	267.7	89.1	178.6	0.93	2.49	255.2	6.42	99.1	1195
B-3	5	3.50	4.10	112.8	52.8	60.1	0.88	2.65	105.5	2.93	95.5	1386
	6	13.00	13.60	226.2	64.3	161.9	0.87	3.04	204.6	6.35	98.1	1263
	7	26.00	26.60	270.6	75.4	195.3	0.88	3.24	247.3	6.36	100.0	1228
	8	56.30	57.10	144.7	56.7	88.0	0.40	2.65	91.8	2.57	94.9	1426
B-4	9	3.50	4.40	167.3	70.5	96.8	0.62	2.58	130.6	3.52	95.6	1318

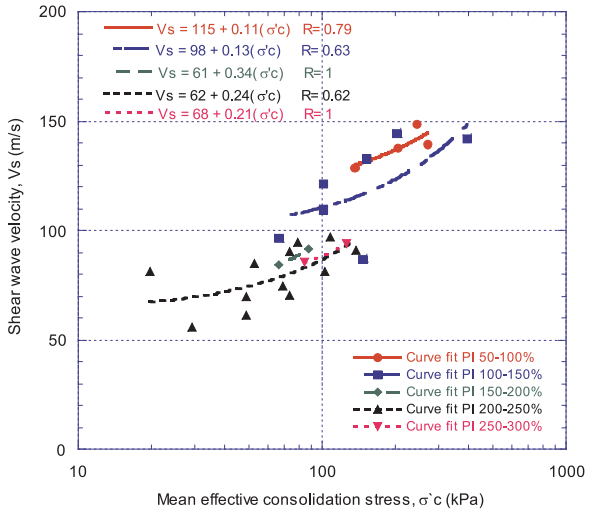

Fig. 6. Variation of shear wave velocity with mean effective stress.

experimental data for "field" conditions to account for sample disturbance and other effects [2] by adjusting these values in 10%. The expected shear wave velocity for each consolidation time (i.e. 5, 10, 30 and 60 year), are shown in Fig. 7.

4. Modulus degradation and damping curves

González and Romo [14] proposed a simplified model to predict the normalized modulus degradation and damping curves obtained in the laboratory performing resonant column and triaxial tests. The model is able to match the shear modulus degradation and damping curves separately. This model is defined by the following expressions:

$$G = (G_{\min} - G_{\max})H_G(\gamma) + G_{\max} \quad (1)$$

$$\lambda = (\lambda_{máx} - \lambda_{\min})H_\lambda + \lambda_{\min} \quad (2)$$

$$H_G = \frac{(\gamma/\gamma_{rG})^{2B_G}}{1 + (\gamma/\gamma_{rG})^{2B_G}} \quad (3)$$

$$H_\lambda = \frac{(\gamma/\gamma_{r\lambda})^{2B_\lambda}}{1 + (\gamma/\gamma_{r\lambda})^{2B_\lambda}} \quad (4)$$

where G_{max} and λ_{min} are the small shear strain shear modulus and damping respectively, these are unique for each soil type. The parameters G_{min} and λ_{max} are the values that reach G and λ before dynamic failure, which is defined as the ultimate shear stress acting on the clay in undrained dynamic conditions, S_{ud}, which led to the sample failure. According to [15], S_{ud} can be estimated as a function of the undrained static shear strength S_u using the following relation:

$$S_{ud} = \frac{M_d(3-M_e)}{M_e(3-M_d)}S_u \quad (5)$$

where M_d is the slope of the dynamic failure envelope expressed also in terms of total stresses, and M_e is the slope of the static failure envelope expressed in terms of the total stresses. For Mexico City clays, the strength determined under dynamic loading, S_{ud}, is larger than the strength under static conditions, S_u. Experimental results indicate that independently of the consolidation trajectory followed and the magnitude of the octahedral consolidation stress, S_{ud}, ranges between 1.20 and 1.40 times S_u. The parameters γ_{rG} y $\gamma_{r\lambda}$ are the reference strains corresponding to 50% of degradation of the shear modulus, and 50% of

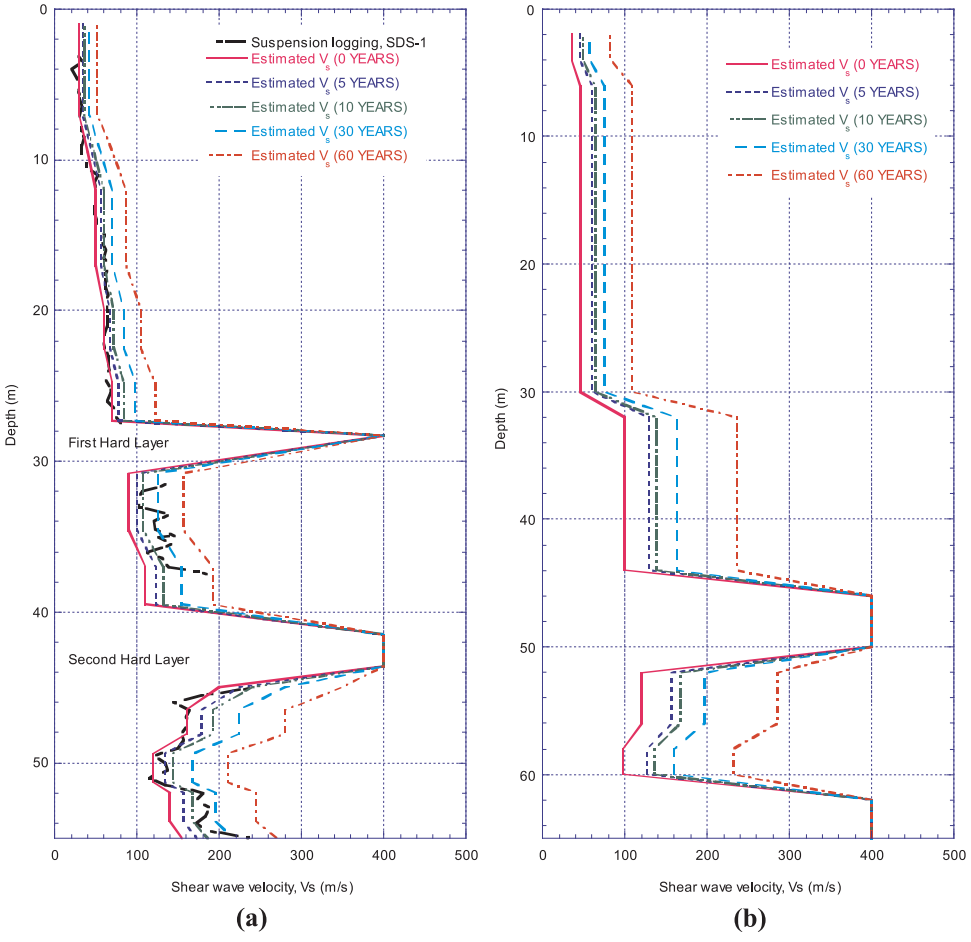

Fig. 7. Shear wave velocity profile evolution (a) Site 1 and (b) Site 2.

Table 2
Parameters used in the analyses for Site 1.

Depth	Gonzalez and Romo's model									FLAC^{3D} (Sig3 model)		
[m]	PI	G_{max}	G_{min}	λ_{max}	λ_{min}	γ_{rG}	$\gamma_{r\lambda}$	B_G	B_λ	a	b	x_0
3.3	165	38.10	2.00	15.00	2.00	0.80	0.80	0.46	0.82	1.00	−0.50	0.01
8.2	270	35.00	1.00	14.00	2.50	1.50	1.50	0.52	0.90	1.00	−0.42	0.20
12.3	194	57.44	1.00	14.00	2.50	1.50	1.50	0.48	0.86	1.00	−0.45	0.20
15.4	202	63.69	1.00	14.00	2.50	1.50	1.50	0.49	0.87	1.00	−0.45	0.20
18.7	137	100.80	2.00	15.00	2.00	0.80	0.80	0.44	0.78	1.00	−0.50	−0.08
24.3	179	96.35	1.00	14.00	2.50	1.50	1.50	0.47	0.84	1.00	−0.46	0.20
	Sand Upper Bound (Seed & Idriss 1970)									0.99	−0.50	−1.15
	Soil PI = 50% (Vucetic & Dobry)									1.01	−0.53	−0.55
	Soil PI = 100% (Vucetic & Dobry)									1.01	−0.50	−0.25

Table 3
Parameters used in the analyses for Site 2.

Depth	Gonzalez and Romo's model									FLAC^{3D} (Sig3 model)		
[m]	PI	G_{max}	G_{min}	λ_{max}	λ_{min}	γ_{rG}	$\gamma_{r\lambda}$	B_G	B_λ	a	b	x_0
4.1	150	35.60	2.00	14.00	2.00	0.80	0.80	0.044	0.81	1.00	−0.44	0.20
8.5	245	29.81	1.00	14.00	2.50	1.50	1.50	0.51	0.90	1.00	−0.45	0.21
12.5	187	56.02	1.00	14.00	2.50	1.50	1.50	0.49	0.82	1.00	−0.45	0.22
14.3	212	73.45	1.00	14.00	2.50	1.50	1.50	0.49	0.84	1.00	−0.43	0.20
18.6	146	84.44	2.00	15.00	2.00	0.80	0.80	0.45	0.79	1.00	−0.50	−0.05
24.4	179	96.35	1.00	14.00	2.50	1.50	1.50	0.47	0.84	1.00	−0.46	0.20
	Sand Upper Bound (Seed & Idriss 1970)									1.01	−0.47	−1.22
	Soil PI = 50% (Vucetic & Dobry)									1.01	−0.53	−0.55
	Soil PI = 100% (Vucetic & Dobry)									1.01	−0.50	−0.25

increase in damping ratio respectively. In this model, these deformations depend only on the plasticity index. The parameters B_G and B_λ are parameters that define the geometry of the curves G–γ and λ–γ respectively, which are a function of the plasticity index (PI). The model parameters used in the analyses are summarized in Tables 2, 3, for sites 1 and 2 respectively.

$$B_G = -2*10^{-6}PI^2 + 0.0014 \quad PI + 0.2846 \tag{6}$$

$$B_\lambda = -7*10^{-6}PI^2 + 0.0038 \quad PI + 0.3282 \tag{7}$$

To estimate the k_o value to be used in the Gonzalez and Romo´s model, the expression (8), proposed by Mayne and Kulhawy [16] was used. This relationship is a function of the over consolidation ratio, OCR, and the friction angle, φ.

$$k_0 = (1 - sen\varphi)(OCR)^{sen\varphi} \tag{8}$$

Based on experimental data, it was established that the clays, at the studied sites included in here, are normally to slightly consolidated, exhibiting values of OCR ranging from 1 to 1.2. For undrained conditions the friction angle for clays is zero, therefore, the k_0 value was equal to 1.

4.1. Gonzales and Romo´s model application

Gonzalez and Romo´s model [14] was used to calculate the normalized modulus degradation and damping curves for each consolidation time. Effective stresses obtained from the numerical simulation were considered to compute the mean effective consolidation stresses for the model. It was assumed that the plasticity index does not change significantly over time. For illustration purposes, the corresponding curves used for initial conditions (i.e. zero years) are presented in Fig. 8, for several mean effective consolidation stresses.

4.2. Seismic environment characterization

The seismic environment at the studied site was characterized through a probabilistic seismic hazard analysis, PSHA, conducted for subduction-fault events as described in Osorio and Mayoral [17]. All seismogenic zones considered in this study were established according to the zonation that Nishenko and Singh [18] carried out for the Mexican subduction zone, which corresponds to where the most damaging earthquakes for Mexico City have been generated. The corresponding source parameters as described by Ordaz and Reyes [19] were obtained from the Mexican catalog of earthquakes prepared by Zuñiga and Guzman [20]. The bayesian statistics procedures described by Rosenblueth and Ordaz [21], and Arboleda and Ordaz [22] were used to derive these parameters. As suggested by Reyes [23], the seismicity of the seismogenic zones was modeled with the modified Gutenberg-Richter recurrence law, to define the exceedance rate of earthquakes with magnitudes larger than 4.5 and lower of 7. In addition, to define the exceedance rate of earthquakes with magnitude larger than 7, the recurrence law for the characteristic earthquake proposed by Ordaz and Reyes [19] was adopted. In this expression it is assumed that the behavior of the characteristic earthquake observed by Singh et al., [24] in the Mexican subduction zone follows a Gaussian distribution. In here, the attenuation relationship proposed by Reyes [23] was used for subduction events, which allows the estimation of the spectral acceleration, S_a, in rock outcrops in Mexico City. This function is the same as that proposed by Joyner and Boore [25]. Once established the earthquakes recurrence models, the seismogenic zones where they occur, and the attenuation law for the studied site, the integral of seismic risk needs to be solved according to the probabilistic approach [26,27]. The risk is evaluated as the probability of exceeding an upper value of the parameter of the ground motion at the site, due to the activity of all seismogenic zones that surround it, and which may contribute to the expected ground motion.

Uniform hazard spectrum, UHS, for three return periods (i.e. 125, 250 and 2475 years) were developed in a nearby rock outcrop (Fig. 9), where the seismological station TXCR was located (Fig. 1), to be able to compare them with measure responses in future research. Only subduction zone earthquakes developed in the Mexican Pacific Coast were considered in the UHS determination. Station TXCR is located at about

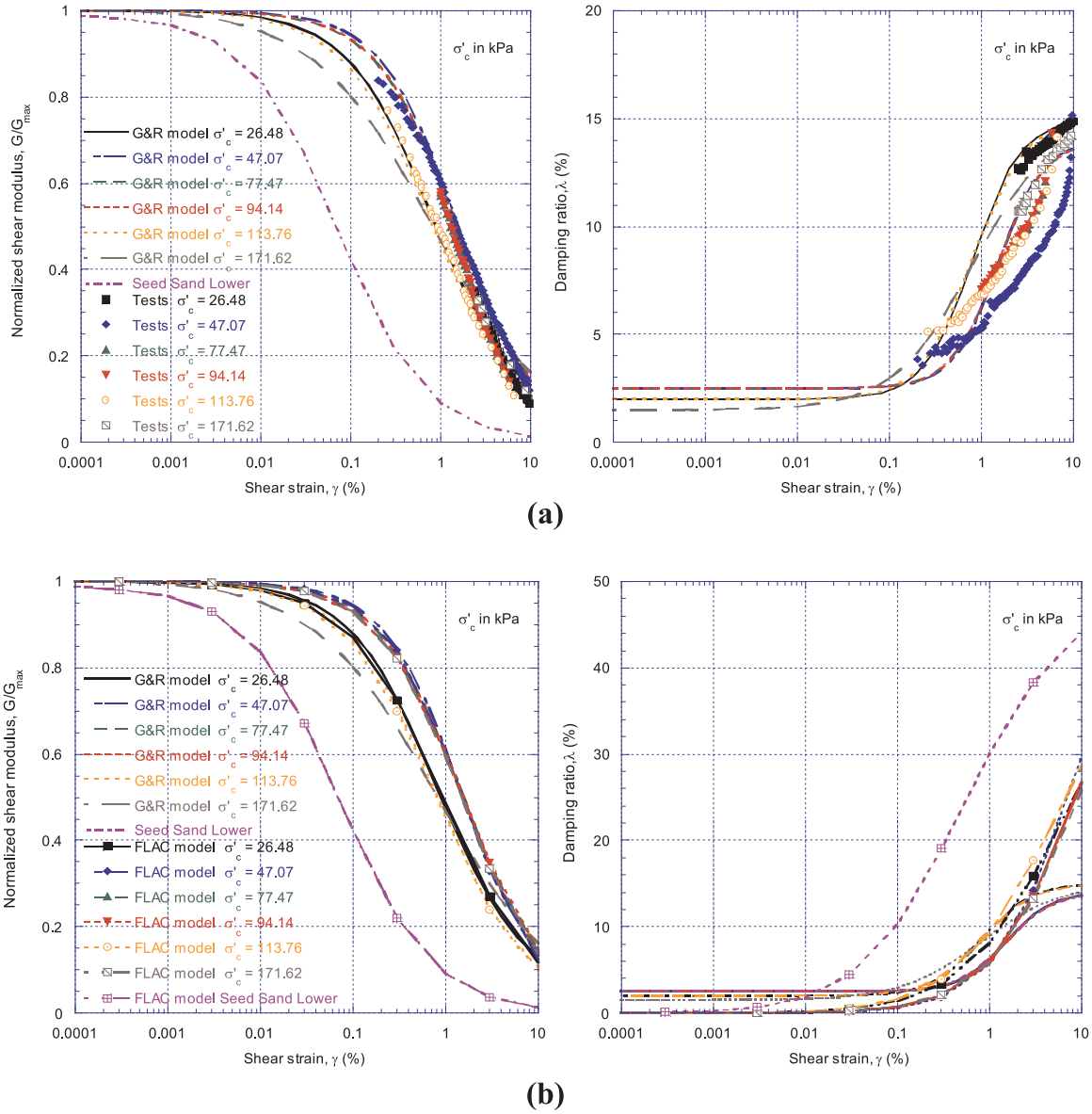

Fig. 8. Modulus degradation and damping curves for initial conditions (zero years) obtained from (a) laboratory testing and Gonzales and Romo´s model for clays, and (b) Gonzales and Romo´s curves fitting with sig3 FLAC^{3D} Model.

18.7 km from the studied site. The return period of 125 years approximately corresponds to the devastating 1985 Michoacan earthquake. The approach followed herein has been validated in previous work [17]. UTM coordinates of the seismological stations located at the site are shown in Table 4. The return period of 250, and 2475 years corresponds to major and extreme earthquakes respectively. As it is well known, the uniform hazard spectra, UHS, is a representation of the relationship between the natural vibration period, T, and spectral acceleration, Sa, for a given exceedance probability associated with a return period.

4.3. Synthetic ground motion

To develop an acceleration time history which response spectrum reasonably matches the design response spectrum for each return period of analysis (i.e. T = 125, 250, and 2475 years), the selected time history, usually called seed ground motion, was modified using the method proposed by Lilhanand and Tseng [28] as modified by Abrahamson [29]. This approach is based on a modification of an acceleration time history to make it compatible with a user specified target spectrum. The modification of the time history can be performed with a variety of different modification models. In doing so, the long period non-stationary phasing of the original time history is preserved. The 5% damped response spectra calculated for the modified time histories are compared with the target UHS in Fig. 9. It can be seen that the response spectrum calculated from the modified time histories reasonably match the target spectrum. The seed and synthetic ground motions are shown in Fig. 10. The seed is a long duration record (i.e. 175 s) typical of the Pacific Coast subduction zone, measured at the station TACY during the 1985 Michoacan earthquake, located on firm soil (i.e. very stiff silty sand and sandy silt). This acceleration time history is available in the Strong Ground Motion Mexico Database.

5. Site response analysis

Initially for completeness, the computer code SHAKE [6] was used to conduct the 1D equivalent linear site response analysis, to have an estimation of the expected results in the free field for moderate to medium ground shaking levels (i.e. return periods of 125 and 250 years). Then, a fully non-linear site response analysis was carried out

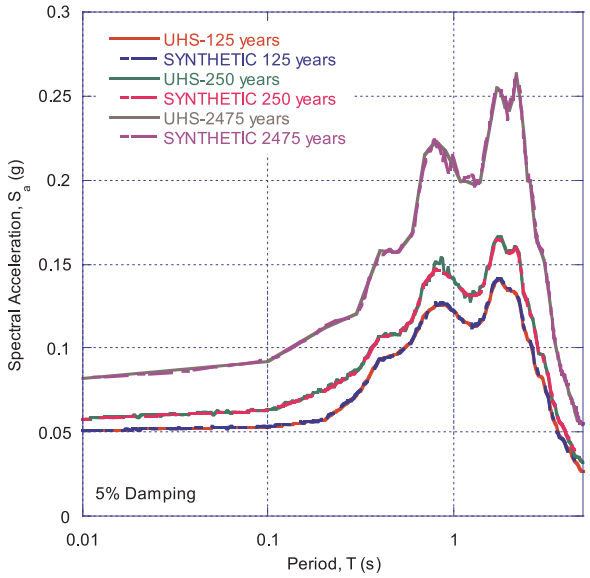

Fig. 9. Computed uniform hazard spectra at TXCR and synthetic ground motion response spectra.

Table 4
UTM coordinates of the seismological stations.

Stations	UTM coordinates	
TXSO	x = 498,007 m E	y = 2,165,005 m N
TXS1	x = 502,827 m E	y = 2,155,384 m N
TXS2	x = 502,419 m E	y = 2,155,267 m N
TXCH	x = 505,248 m E	y = 2,148,407 m N
TX5B	x = 503,148 m E	y = 2,155,046 m N
T4S3	x = 503,114 m E	y = 2,155,021 m N

using the program FLAC^{3D} [30], to further study soil nonlinearities. The importance of accounting for nonlinear effects on ground motion attenuation as well as frequency content modification during strong shaking has been established in the past by several authors for both site response [31–34], and seismic soil-structure interaction analyses [35–38]. The finite differences model of the free field has a depth of about 62 m for the initial soil conditions prevailing in Site 1 (i.e. right after building construction), and a square section of 10 m by 10 m (Fig. 11). A similar model was prepared for Site 2. The free field boundaries implemented in FLAC^{3D} were used along the edges of the model. A rigid base was considered at the bottom of the model, to simulate the large dynamic impedance contrast existing at the site, in which a low shear wave velocity clay overlaid a high shear wave velocity bedrock. This model was calibrated against the results obtained with the program SHAKE, for a return period of 125 and 250 years. Similar calibrations have been conducted by [39,40].

Although several constitutive models have been developed to account for nonlinearities in low plasticity clays and sands [40,41], there is a lack of enough experimental data to develop and calibrate a reliable constitutive model for high plasticity clays. Thus, the practical-oriented hysteretic model available in FLAC^{3D} [30] denominated as "sig3" was used to approximately deal with both modulus stiffness degradation and damping variation during the seismic event. This model considers an ideal soil, in which the stress depends only on the deformation and not on the number of cycles, with these assumptions an incremental constitutive relationship of the degradation curve can be described by $\tau_n/\gamma = G/G_{max}$, where τ_n is the normalized shear stress, γ is the shear strain and G/G_{max} the normalized secant modulus. The sig3 model is defined according to Eq. (9):

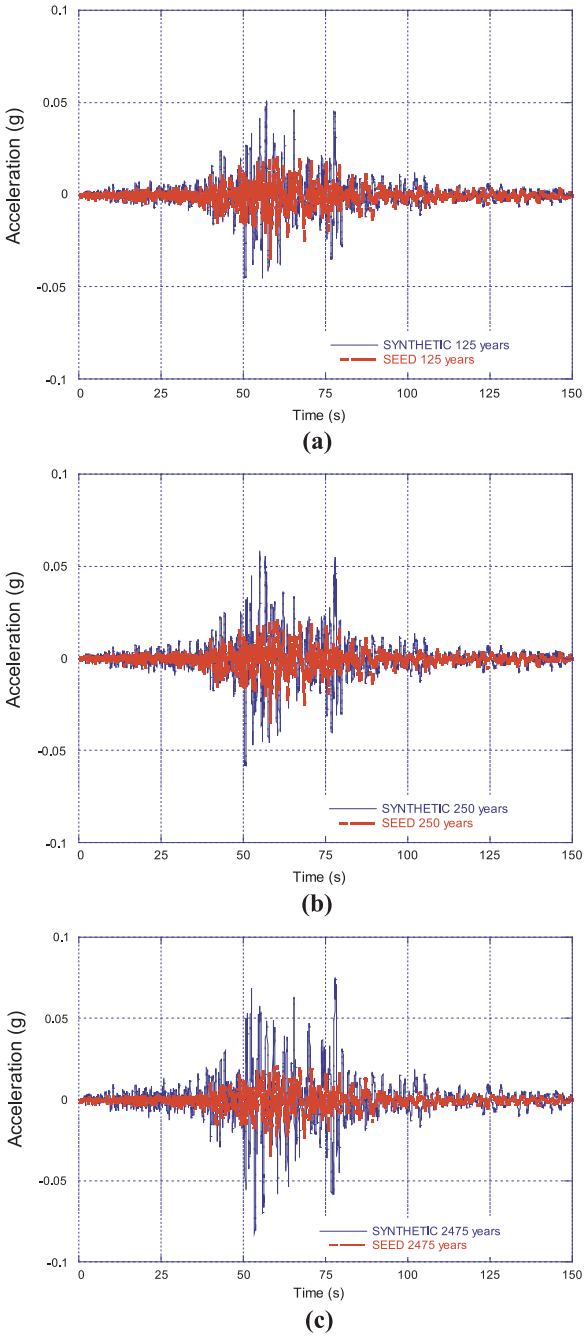

Fig. 10. Seed and synthetic time histories for a) 125 years, b) 250 years and c) 2475 years.

$$G/Gmax = \frac{a}{1+exp\left(-\frac{L-x_0}{b}\right)} \tag{9}$$

where L is the logarithmic strain defined as $L = \log_{10}(\gamma)$, and the parameters a, b, and $\times_0$, used by the sig3 model were obtained by an iterative approach, in which the modulus degradation curves obtained from Gonzales and Romo´s model [14] were fitted with the model equations. The corresponding damping is given directly by the hysteresis loop during cyclic loading. For the cases studied herein, the parameter "a" ranges from 0.99 to 1.00, "b" from −0.43 to −0.6, and "x_0" from −1.15 to 0.21. Tables 2, 3, summarizes the parameters used in the analyses for several depths. The corresponding G/G_{max} fitting curves are presented in Fig. 8b.

It is important to point out that Eqs. (1)–(7) described a simplified model proposed by Gonzalez and Romo [14], driven by the plasticity

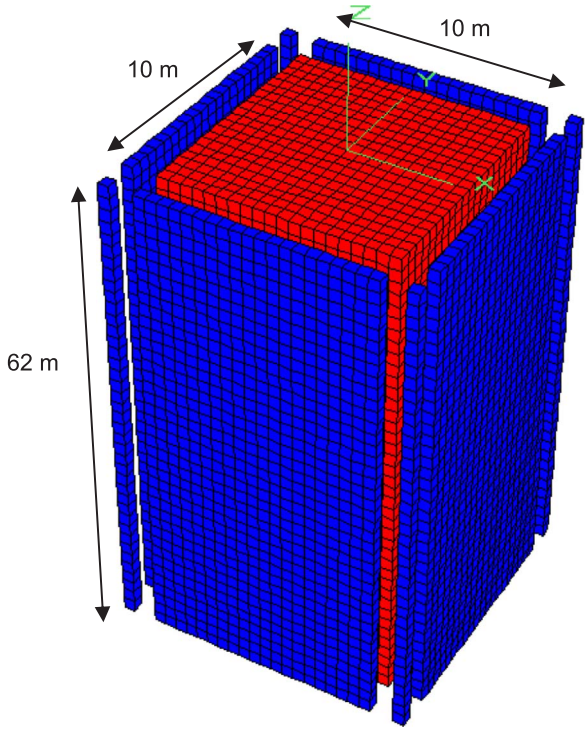

Fig. 11. Three-dimensional finite difference model.

index, PI, to fit experimental normalized modulus degradation G/G_{max} and damping curves obtained from resonant column and cyclic triaxial test conducted in high plasticity clays. This allowed to characterize the dynamic response of soil layers, where experimental information was not available. Eq. (9) is a massing type model that allows to account for soil nonlinearities in a simplified fashion, by following the evolution of the normalized shear modulus as a function of the shear strain, during the time domain analysis. Accordingly, to find the ground motions in the underlying bed rock to be used in the time domain site response analyses, the synthetic ground motion computed at the rock outcrop was deconvolved with the program SHAKE to the hardlayer found at the base of the soil profile. The seismic excitation at the base of the FLAC^{3D} model, is a function of the impedance ratio between the stiff clay found at the base of the model (i.e. about 60 m depth), and the assumed half space. This changes were minimal, because for the stiff clay layers found at 60 m depth, the variation of V_s over time is very small, considering the minor changes in effective stresses developed at that depth.

5.1. Pore pressure evolution with time

Static stress-strain and pore pressure conditions for each time are the starting point for the dynamic analysis. These included state of stresses, ground settlements and soil layering configuration. Ground settlements and changes in layering configuration can be estimated solving the diffusion equation [30] for the pore pressure, p, given by:

$$\frac{\partial p}{\partial t} - c\frac{\partial^2 p}{\partial z^2} = 0 \tag{10}$$

where $C = k/S$, $S = \frac{1}{M} + \frac{\alpha^2}{\alpha_1}$ is the storage coefficient and k the soil permeability, $\alpha_1 = K + \frac{4}{3}G$. M is the Biot modulus, α is the Biot coefficient, and K and G are the bulk and shear modulus respectively. Eq. (10) considers the variation of the effective vertical stress σ_{zz} constant with time, and is derived for the boundary conditions: $p = 0$ at $z = H$, and $\frac{\partial p}{\partial z} = 0$ at $z = 0$. Due to the uncertainties associated with the determination of M, and α, which truly represent field conditions, and the fact that the clays at the site are very fissured and interbedded with very thin silt layers, a practice-oriented uncoupled procedure was used to estimate the ground settlements in the soil deposit, which also allowed for a reduction in computation time. Initially, the evolution of pore pressure withdrawn with water extraction was established based on the available piezometers readings located at several depths (i.e. 9, 18, 31, 38 and 45 m) as depicted in Fig. 3. This figure shows the evolution of normalized measured pore pressure, u, over the initial reading, u_o. Based on these data, empirically-derived equations were used to estimate the expected evolution of the pore pressure over time. Fig. 4, shows the corresponding computed pore pressure distribution with depth for the time of analyses (i.e. 5, 10, 30 and 60 years). Once the expected pore pressure evolution was established, the analytical solution provided by Terzaghi´s theory for one dimensional consolidation, $\Delta H = m_v pH$, where m_v is the volumetric modulus, H layer thickness, and ΔH the corresponding layer deformation, was used to evaluate the corresponding expected settlements for each consolidation time. The parameter m_v was characterized based on series of one-dimensional consolidation tests conducted in undisturbed samples retrieved in both the upper clay formation, UCF, (i.e. depths ranging from 1 to 28 m, approximately), and the lower clay formation (i.e. depths ranging from 32 to 62 m, approximately). As previously mentioned, from the one-dimensional consolidation tests, the variation of the volumetric modulus, m_v, with the mean effective consolidation stress was established for both the UCF and LCF, as depicted in Fig. 5. Thus, to compute the ground settlements for each consolidation time (i.e. 5, 10, 30 and 60 years), instead of solving the diffusion equation, a subroutine was implemented in FLAC^{3D} to impose incrementally the state of stresses associated to each consolidation time according to the pore pressure distributions depicted in Fig. 4. For each pore pressure expected decrement due to water extraction, the m_v was modified according to Fig. 5, and the corresponding increment in ground settlements were calculated using the expression $\Delta H_i = m_{vi} p_i H_i$ at each nodal point, and the large strain formulation available in FLAC^{3D}. Thus, both changes in soil compressibility, as well as in soil layering configuration during regional subsidence due to water extraction was accounted for in the analyses. It can be easily verified that this simplified methodology leads to similar results as those reached solving the diffusion equation [42]. A similar approach was employed to compute the settlements associated with the dissipation of excess pore pressure due to building loading. The excess pore pressure distribution in the in the ground was obtained directly from FLAC^{3D} considering undrained conditions, and again, the expected settlements were calculated using the expression $\Delta H_i = m_{vi} p_i H_i$ at each nodal point. These settlements were added to those corresponding to water extraction for each consolidation time, assuming that most of the ground settlements due to excess pore pressure associated to building loading will occur in the first five years. This is in agreement with the fact that the clays are very fissured and interbedded with thin silt lenses, therefore, the rate of settlements is expected to be larger at the beginning of the consolidation process. The computed consolidation settlements are in agreement with those observed in both the free field and building-loaded areas adjacent to the studied sites, and other similar ground conditions zones found in Mexico City [43].

Fig. 12 shows the initial stresses state, computed right after the construction was completed. The so-called analytical-solution curve was obtained subtracting the total vertical stresses acting at the studied sites minus the corresponding pore pressure for initial conditions (i.e. 0 years), and compared with the ones obtained with FLAC^{3D} to ensure that the initial stress conditions were properly captured. Both soil consolidation mechanisms 1) settlements due to the dissipation of excess pore pressure generated by the building load, and 2) regional subsidence effects, due to ground water extraction, are considered in the settlement computation. For zero years the initial state stress depicted in Fig. 12 was considered in the simulation. These are related to the three-dimensional free field model shown in Fig. 11. Thus, the building load is not yet applied to the model. The accumulated displacements of each layer contribute to the settlement evolution on the

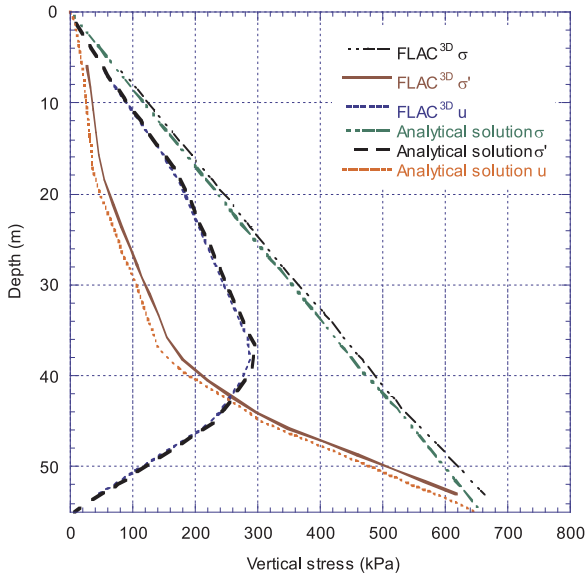

Fig. 12. Initial stresses state.

surface. The cumulative increase of deformations for sites 1 and 2 are shown in Fig. 13.

5.2. Free field response

Site response analyses were carried out for each static ground conditions, accounting for changes both in the dynamic properties, as well as in soil thickness, for the two studied sites. To further revise the accuracy of the model, comparison of the computed responses for initial conditions (0 years) were carried out using the program SHAKE and FLAC^{3D}, for moderate to large ground shaking levels (i.e. return periods of 125 and 250 years). The results for Site 1 are presented in Fig. 14a and b, for a return period of 125 and 250 years respectively. As can be noticed, there is a good agreement between the response computed with SHAKE and FLAC^{3D} for a low return period (125 yeas), due to the quasilinear range that the high plasticity Mexico City Clay exhibit even for shear strains as long as 0.3%, as previously pointed out. Thus, only a small degree of soil nonlinearities is expected to occur. For the return period of 250 years, there is a reduction of the spectral ordinates and a slightly fundamental period shifting to the right due to soil nonlinearities.

Fig. 15 presents the normalized spectral acceleration, Sa/PGA, computed at the free field for sites 1 and 2. As can be seen, both amplification and frequency content are function of the consolidation time. The trends seem to indicate that the amplification decreases in the firsts 10 years, but for 30 and 60 years, there is an amplification, as well as a period elongation from 1.9 to 2.5 s Fig. 16 shows the response computed for 5, 10, 30 and 60 years, normalized with respect to that obtained for initial conditions (i.e. $\frac{(Sa(T)/PGA)_{i\ years}}{(Sa(T)/PGA)_{0years}}$). Table 5 shows the evolution of fundamental elastic periods for each consolidation time. As can be noticed the fundamental elastic (i.e. soil stiffness does not change with the shear strain amplitude) periods tend to decrease when the consolidation time increases. Similarly, Table 6 shows the fundamental periods obtained from the transfer functions computed between the responses at surface and bedrock as depicted in Fig. 17. This table also includes the periods at which the maximum spectral accelerations, S_a, are presented (Fig. 15). It can be noticed that consolidation changes both the frequency content and spectral accelerations. For site 1, after 5 and 10 years of ground consolidation, the maximum response has migrated to the right and the higher spectral ordinates are reached at 2.3 s. Thus, soil nonlinearity prevails as the elastic period shifts towards 1.8 s, which corresponds to the period where the seismic excitation has

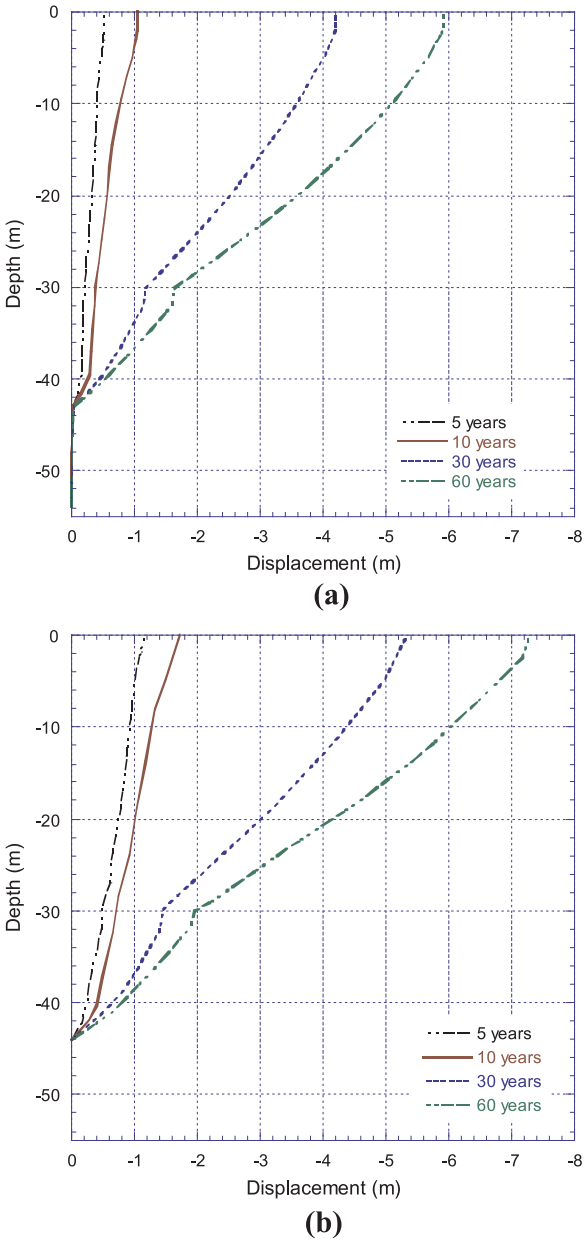

Fig. 13. Settlements over time for (a) Site 1 and (b) Site 2.

its energy concentrated (i.e. 0.8 and 1.8 s). Ground amplification initially tends to increase but soil nonlinearities reduce the maximum spectral accelerations and elongate both the fundamental periods, as well as the periods at which the maximum spectral accelerations are presented. After these critical years, when reaching 30 and 60 years of consolidation, the dynamic properties and layering thickness have drastically changed, so the fundamental elastic period has reduced down to 1.55 and 1.26 s respectively. Thus, a reduction in spectral accelerations is observed. The same trend can be seen for Site 2. The period associated to the maximum spectral acceleration moves to the right for 5, 10 and 30 years mostly due to nonlinear effects. However, after 60 years of consolidation, the fundamental elastic period has gone down to 1.10, the fundamental period has gone down to 1.37 s, and the maximum spectral acceleration has reduced accordingly.

6. Seismic soil-structure interaction

A three dimensional finite difference model was developed with the program FLAC^{3D} [30], using the large strain formulation available in

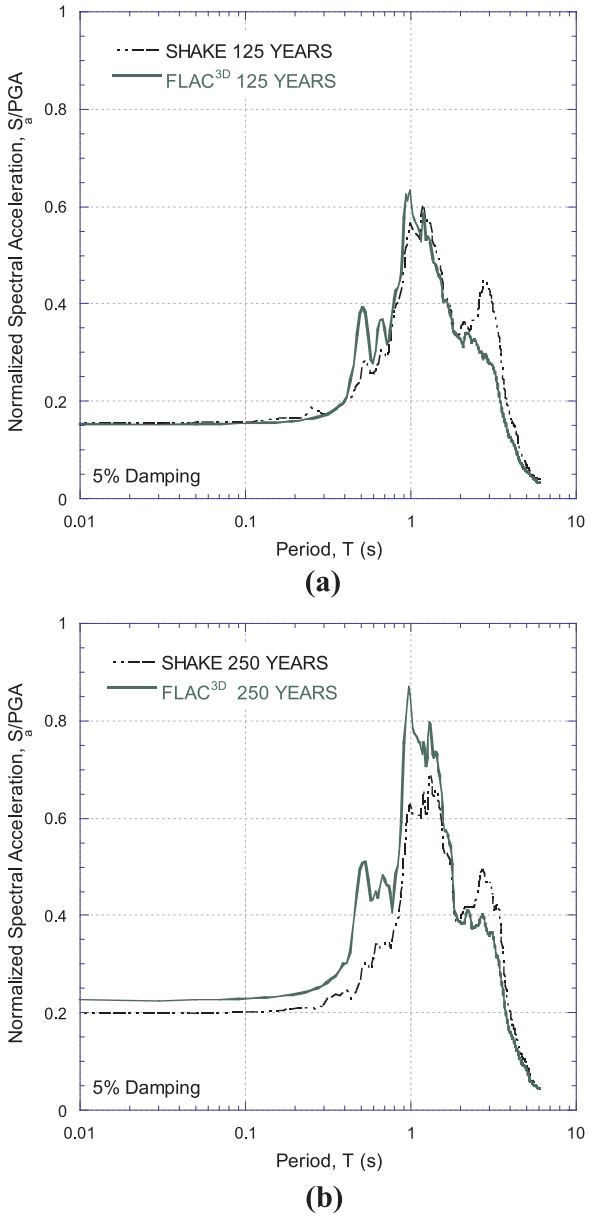

Fig. 14. Results of the site response analysis for the return period of (a) 125 and (b) 250 years (Site 1).

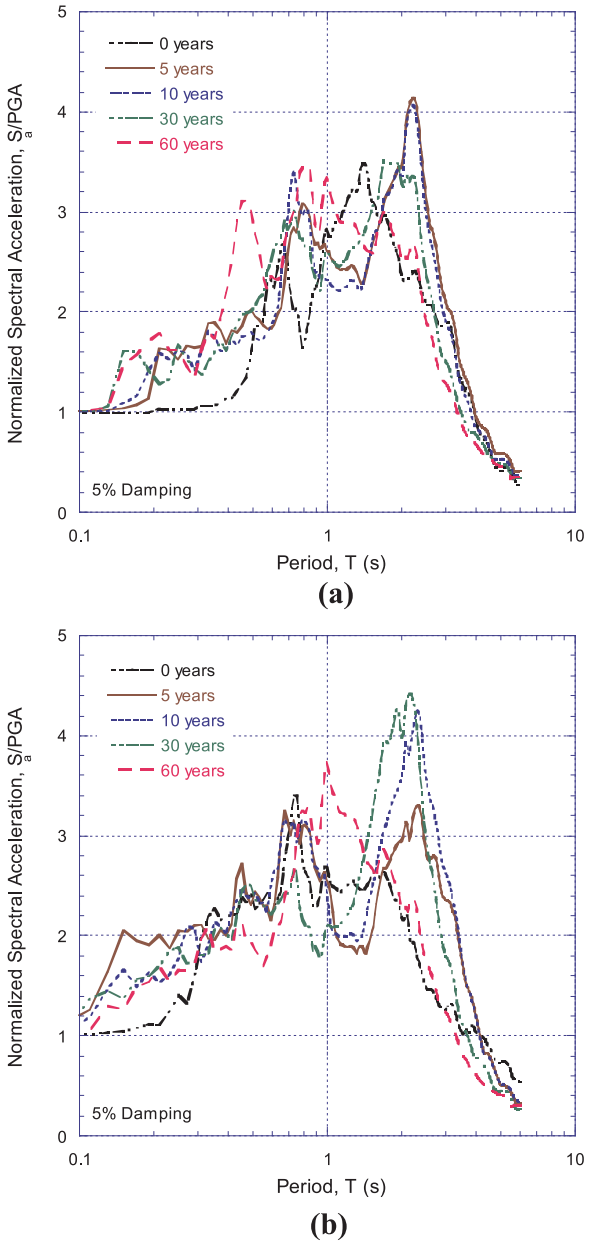

Fig. 15. Normalized response spectra of the non-linear analysis calculated with FLAC^{3D} for (a) Site 1 and (b) Site 2.

the software, to analyze the seismic soil-structure interaction system response. The stress-strain relationship of the soil was assumed elasto-plastic, following the Mohr-Coulomb failure criterion. In the finite difference model the columns and slabs, were modeled with beam and shell elements respectively. Fig. 18 shows the building dimensions and the transversal section of the columns and beams considered. The thickness slab was assumed as 0.15 m. Table 7 summarizes the corresponding material properties considered in the numerical model. The thickness of the element was selected based on the geometry and sizes of both structural elements and soil layers. However, as it is well known, numerical distortion of the propagating wave can occur in a dynamic analysis as a function of the modeling conditions [30]. Therefore, both the frequency content of the input wave and the wave speed characteristics of the system will affect the numerical accuracy of wave transmission. In the case studied herein, it was considered the recommendation provided by Kuhlemeyer and Lysmer [44], regarding the spatial element size, Δl, to accurately represent wave transmission through the numerical models employed. Therefore, Δl, was kept smaller than one-fifth of the wavelength associated with the highest frequency component of the input wave that contains appreciable energy, f_{max} (i.e. $\Delta l \leq \lambda/5$). The shortest wavelength λ is obtained from $\lambda = Vs/f_{max}$. For the problem at hand, the smallest average shear wave velocity Vs of the two studied sites in the upper 28 m of clay was about 30–40 m/s for initial conditions (i.e. 0 years), as can be seen in Fig. 7, and the highest significant frequency of the excitation where the energy is concentrated is around 2–3 Hz. Thus, λ ranges approximately between 10 and 13 m. Moreover, the maximum spectral responses of the excitation are presented even at lower frequencies (i.e. 1.3 and 0.6 Hz), as depicted in Fig. 9. Hence, a Δl of 2 m was deemed appropriated. Using similar meshes with element sizes of 2 m in previous research, a good agreement has been obtained between finite difference models developed with FLAC^{3D} and SHAKE for low to moderate levels of shaking, using equivalent linear properties [12,45]. SHAKE models predictions have been, in turn, previously compared against measured responses showing also a good agreement [46]. Furthermore, due to the characteristics of the seismogenic subduction zone, and the distance between the zone of energy release and the studied site (i.e. about

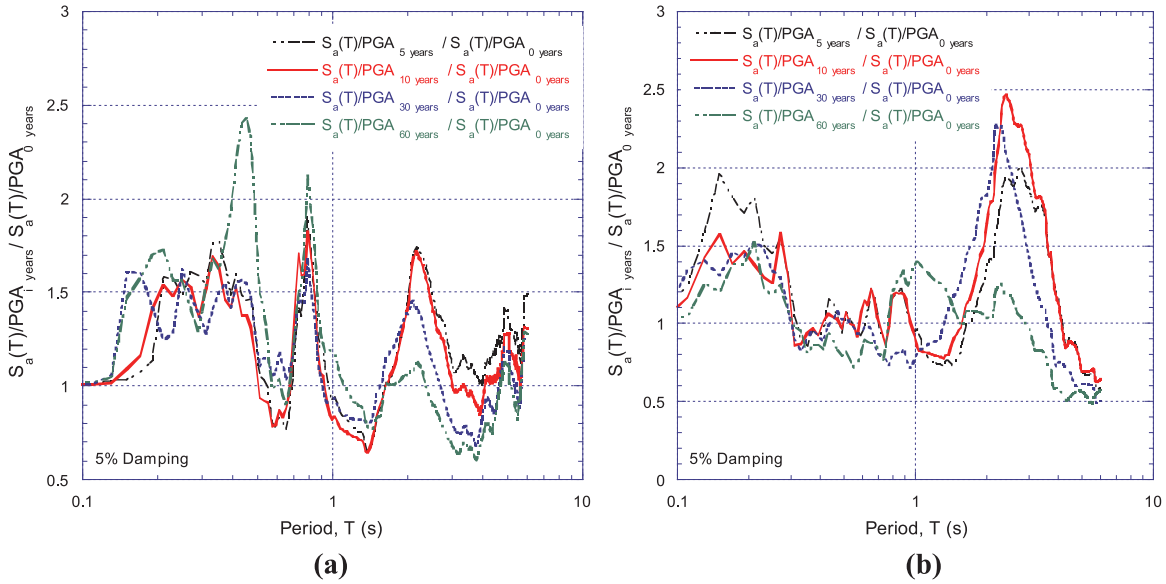

Fig. 16. Normalized response spectra of the non-linear analysis calculated with FLAC^{3D} for (a) Site 1 and (b) Site 2.

Table 5
Evolution of fundamental elastic periods at free field.

Years	Site 1 T [s]	Site 2 T [s]
0	2.09	2.01
5	1.94	1.74
10	1.83	1.66
30	1.55	1.42
60	1.26	1.09

Table 6
Evolution of fundamental periods, and periods at which the maximum spectral acceleration are reached at free field.

Years	Site 1		Site 2	
	T [s]	A[a]	T [s]	A[a]
0	1.44 (1.39)	3.41	0.73 (0.73)	3.41
5	2.27 (2.35)	4.10	2.32 (2.41)	3.31
10	2.22 (2.29)	4.06	2.31 (2.29)	4.25
30	1.76 (2.21)	3.50	2.15 (2.27)	4.42
60	1.00 (1.53)	3.35	1.00 (1.37)	3.74

[a] A is amplification ratio S_a/PGA, ( ) fundamental periods.

380 km), it is not expected to have any dynamic input with a high peak velocity and short rise-time. Thus, no further filtering of high frequency components of the time histories was required. The box foundation is excavated to a depth of 5 m. The structural damping for the building and foundation was defined using a Rayleigh-type damping, assuming 5%, at the fundamental frequencies of the soil-structure system. The model has 10,360 solid elements, 12,065 nodes, 1577 elements and 759 nodes, as depicted in Fig. 19. The soil layers are identified as follows: 1) upper crust, UC, 2) upper clay formation, UCF, 3) first hard layer, FHL, 4) lower clay formation, LCF, and 5) second hard layer, SHL. The soil-structure system seismic response was monitored at the control points depicted in Fig. 20. Control points depths are shown in Table 8. To reduce computation time, several size meshes were tried out until finding the optimum dimensions, in which free field conditions were reached at the end, as can be noticed in the contour plots of static initial stresses depicted Fig. 21.

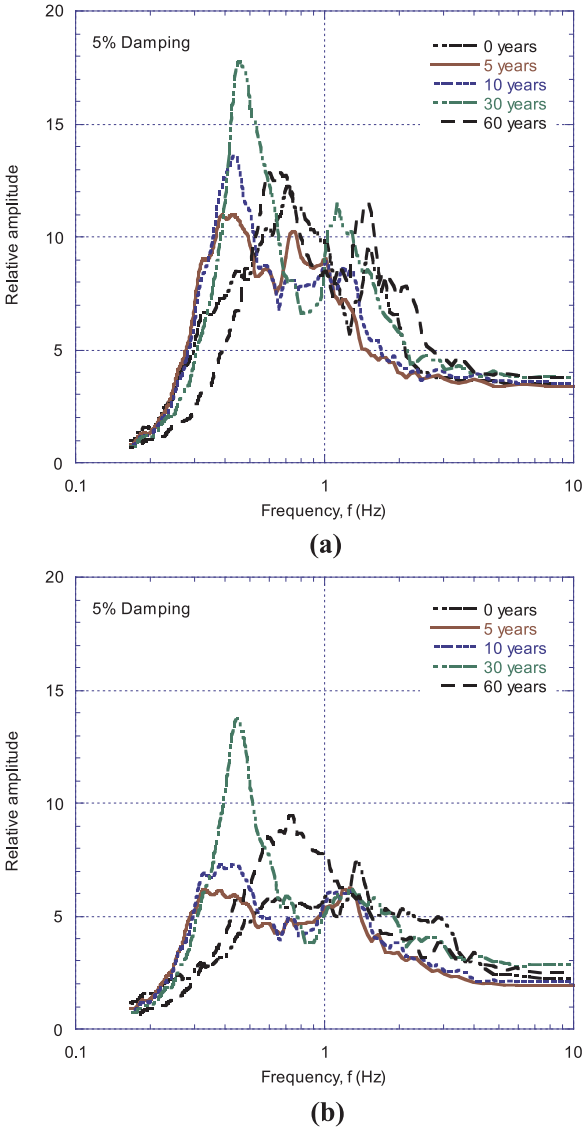

Fig. 17. Transfer functions surface/bedrock for (a) Site 1 and (b) Site 2.

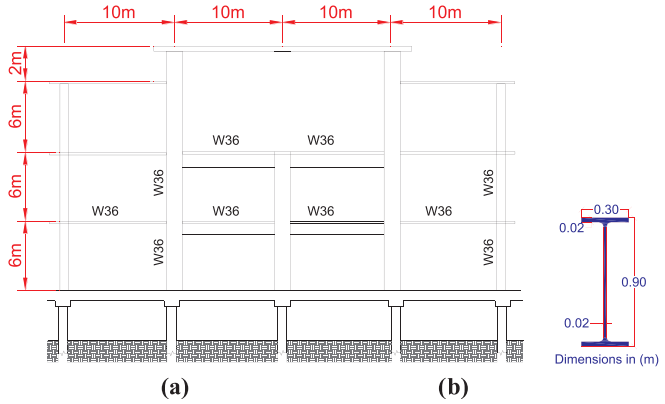

Fig. 18. (a) Elevation view of the analyzed building and (b) W36 × 135 cross section.

Table 7
Structural material properties.

Section	Material	E [GPa]	[MPa]	ν
Column	Steel	206.84	fy = 450	0.29
Beam	Steel	206.84	fy = 450	0.29
Slab	Concrete	24.25	f 'c = 24	0.20

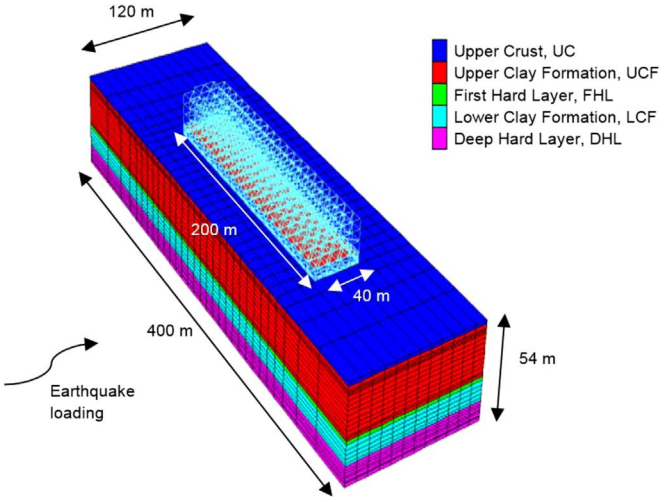

Fig. 19. 3D model for the soil-structure analysis.

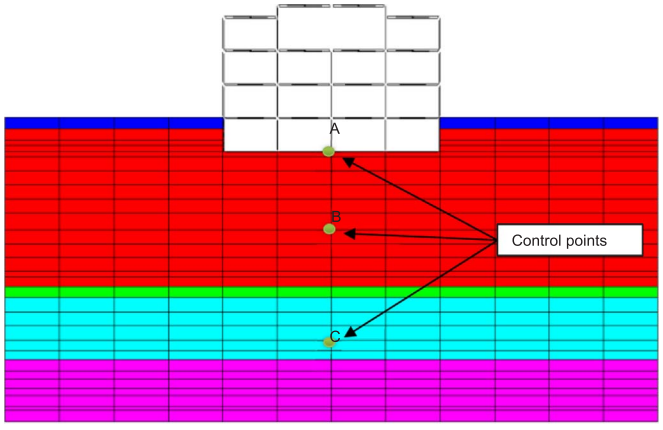

Fig. 20. Control points locations in the 3D model (without scale).

6.1. Static behavior

To assess the effect that ground consolidation has in the seismic soil-structure-interaction response, the total settlements generated for each analysis time considered (i.e. 5, 10, 30 and 60 years) were obtained. Ground movements due to 1) elastic settlements due to weight of the structure applied right after the completion of the building construction, 2) consolidation settlement due to the dissipation of the excess pore pressure generated by the building weight, and 3) regional consolidation due to water extraction were computed. Again, once the expected pore pressure evolution was established, the analytical solution provided by Terzaghi´s theory for one dimensional consolidation, $\Delta H = m_v p H$, where m_v is the volumetric modulus, H layer thickness, and ΔH the corresponding layer deformation, was used to evaluate the corresponding expected settlements for each consolidation time. The parameter m_v, was characterized based on series of one-dimensional consolidation tests conducted in undisturbed samples retrieved in both the upper clay formation, UCF, (i.e. depths ranging from 4 to 36 m), and the lower clay formation (i.e. depths ranging from 40 to 57 m). From the one-dimensional consolidation tests, the variation of the volumetric modulus, m_v, with the effective confining stress was established for both the UCF and LCF as depicted in Fig. 5. Figs. 22–25 shows the total settlements computed after each consolidation time of analysis (i.e. 5, 10, 30 and 60 years) at Site 1. The shape of the distribution of consolidation settlements changes over time due to the regional subsidence associated with groundwater withdraw caused by ground water extraction. Initially, the settlement distribution is control mostly by the consolidation process associated to the dissipation of the excess pore pressure due to the building load. Then, for medium and long term conditions, the settlements tend to be more uniform, and the subsidence effect due to ground water extraction prevails in the ground settlements configurations. Table 9 shows the total displacements at the foundation center and the free field, along with the corresponding differential settlement. It can be noticed that despite the large settlement amount expected at 30 years due to ground consolidation (i.e. around 4.20 m), the differential settlement is negligible. Thus, the soil settlement is almost uniform. A similar conclusion is withdrawn for 60 years, where the total settlements is around 5.50 m, but the differential settlement is quite small (i.e. 0.05 m).

6.2. Seismic response

Seismic soil-structure interaction analyses were carried out for current conditions and after 5, 10, 30 and 60 years of ground consolidation. Changes in dynamic properties and soil profile configuration due to soil consolidation were accounted for, as well as soil nonlinearities. Normalized response spectra with respect to PGA at the control points A, B and C, are depicted in Fig. 26 for both studied sites. Similarly, Fig. 27 shows the response computed for 5, 10, 30 and 60 years, normalized with respect to that obtained for initial conditions (i.e. $\frac{(Sa(T)/PGA)_{i\ years}}{(Sa(T)/PGA)_{0years}}$). Control points A, B and C are located below the foundation building as indicated in Fig. 20, and Table 8. The static conditions for each consolidation time were the starting point of the dynamic analyses. As can be noticed, both frequency content and spectral accelerations amplitudes change over time. The overall response of the soil-structure system for sites 1 and 2 is mostly dominated by the structure and foundation stiffness, which reduces the fundamental period of the soil-structure system T_{ss}. For Site 1 T_{ss} ranges between 0.68–1.32 s and for Site 2 between 0.46 and 1.08 s at control point A, as summarized in Tables 10, 11 respectively. The structural response is similar to that observed in the free field. When the fundamental elastic period gets closer to the periods in which most of the energy of the excitation is concentrated (i.e. 0.8 and 1.8 s), the ground motion amplifies, and thus the soil nonlinearity shifts the fundamental period of the soil-structure system to the right, and the spectral

Table 8
Control points heights.

Height [m]	Control point
−5.00	A
−20.00	B
−41.50	C

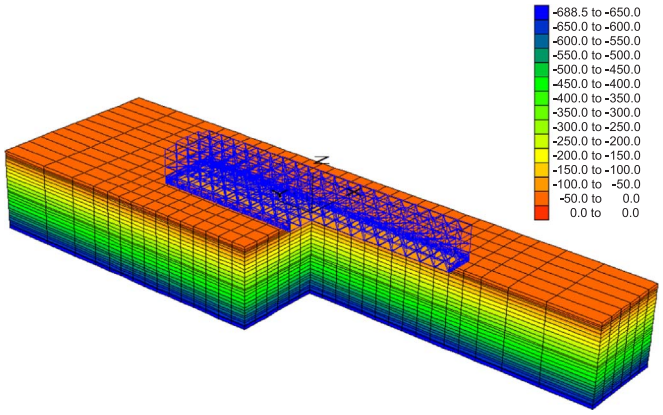

Fig. 21. Initial static total stress distribution (in kPa).

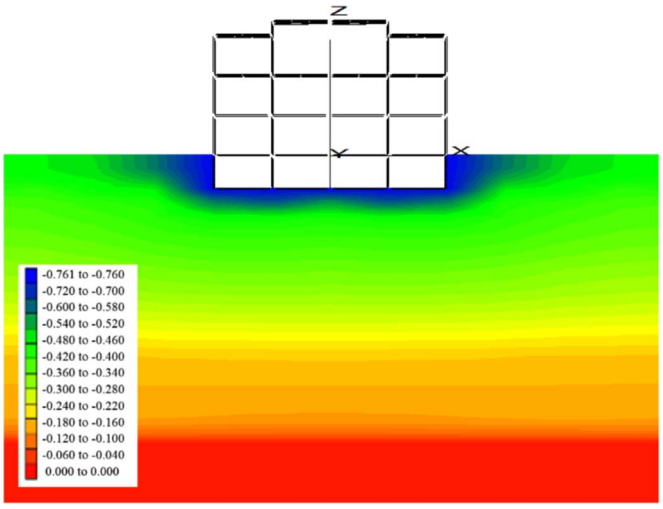

Fig. 22. Total settlements after 5 years in site 1 (in meters).

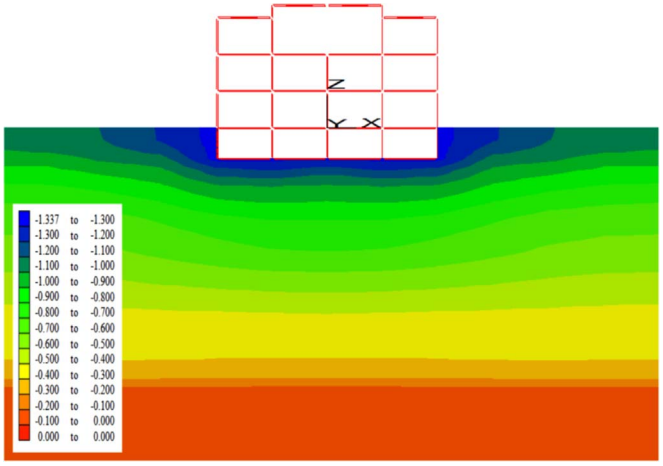

Fig. 23. Total settlements after 10 years in site 1 (in meters).

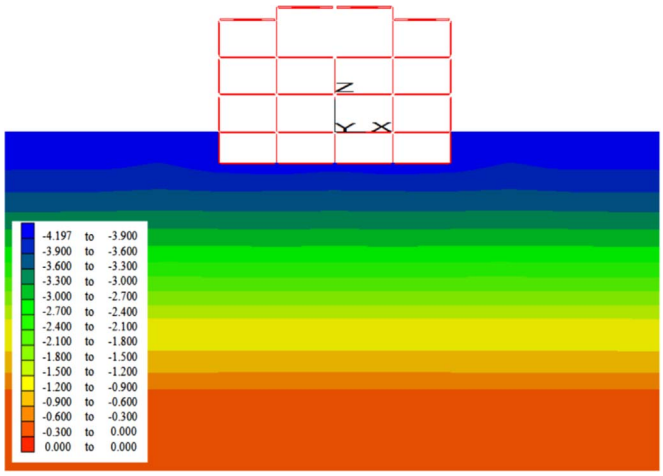

Fig. 24. Total settlements after 30 years in site 1 (in meters).

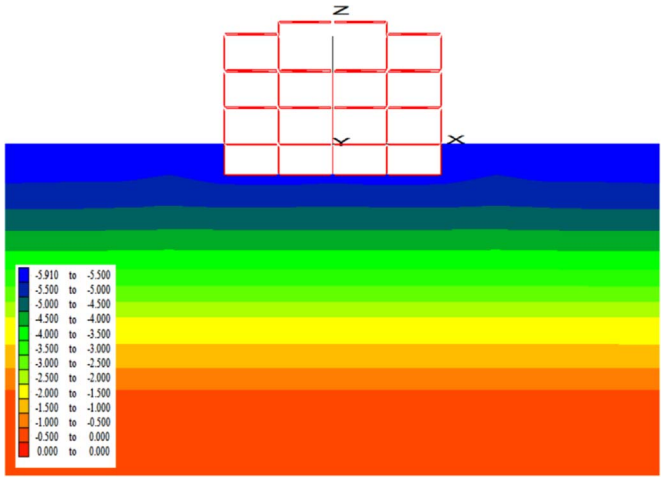

Fig. 25. Total settlements after 60 years in site 1 (in meters).

Table 9
Differential settlements in meters.

Building foundation (at center)	Free field	Differential
−0.75	−0.49	−0.26
−1.30	−0.99	−0.31
−3.90	−3.96	0.06
−5.50	−5.55	0.05

acceleration reduces slightly. Thus, for Site 1 at 5 and 10 years, the nonlinear soil behavior controls the soil-structure seismic response, and the period at which the maximum spectral acceleration occurs moves to the right, and the spectral ordinates are amplified around a fundamental period of 1.45 s, with respect to those obtained considering ground conditions at zero years. After 30 years, the soil gets stiffer. Shear wave velocity distribution increases and the soil thickness decreases. Thus, the elastic fundamental period of the soil deposit goes down, reducing the ground motion amplification. Therefore, the effect of soil nonlinearities is not significant, and the fundamental period of the soil-structure system moves towards 1.22 s. For a consolidation time of 60 years, the elastic fundamental period gets closer to the lower period at which the energy of the excitation is concentrated (i.e. 0.8 s), and also to the fundamental period of the structure on rigid base, T_{sr} (i.e. around 1 s), leading to a large amplification of the soil-structure system response for periods close to 1 s, with the corresponding period elongation due to soil nonlinearities.

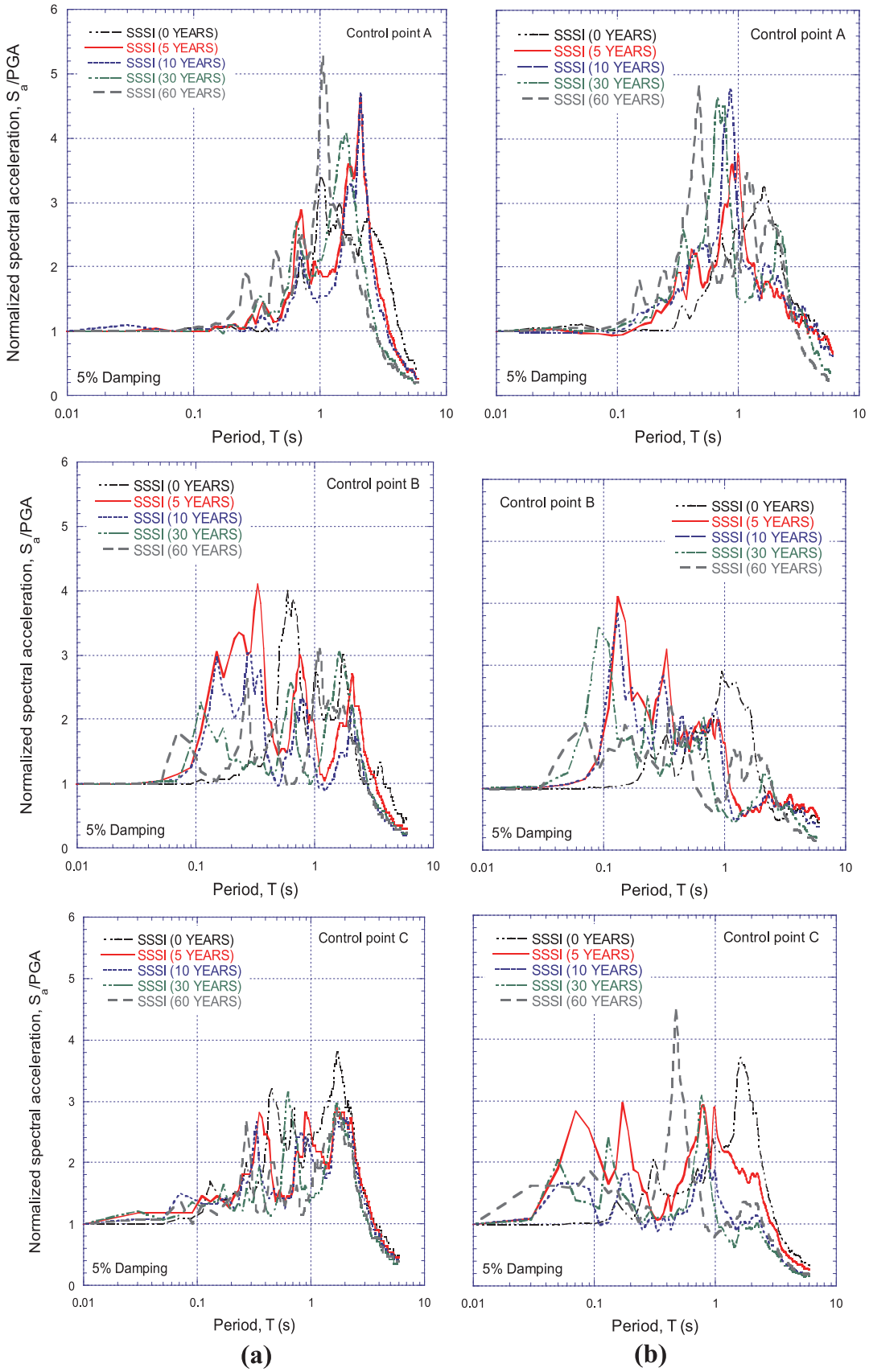

Fig. 26. Evolution of the response spectra with time in control point A, B and C for (a) Site 1 and (b) Site 2.

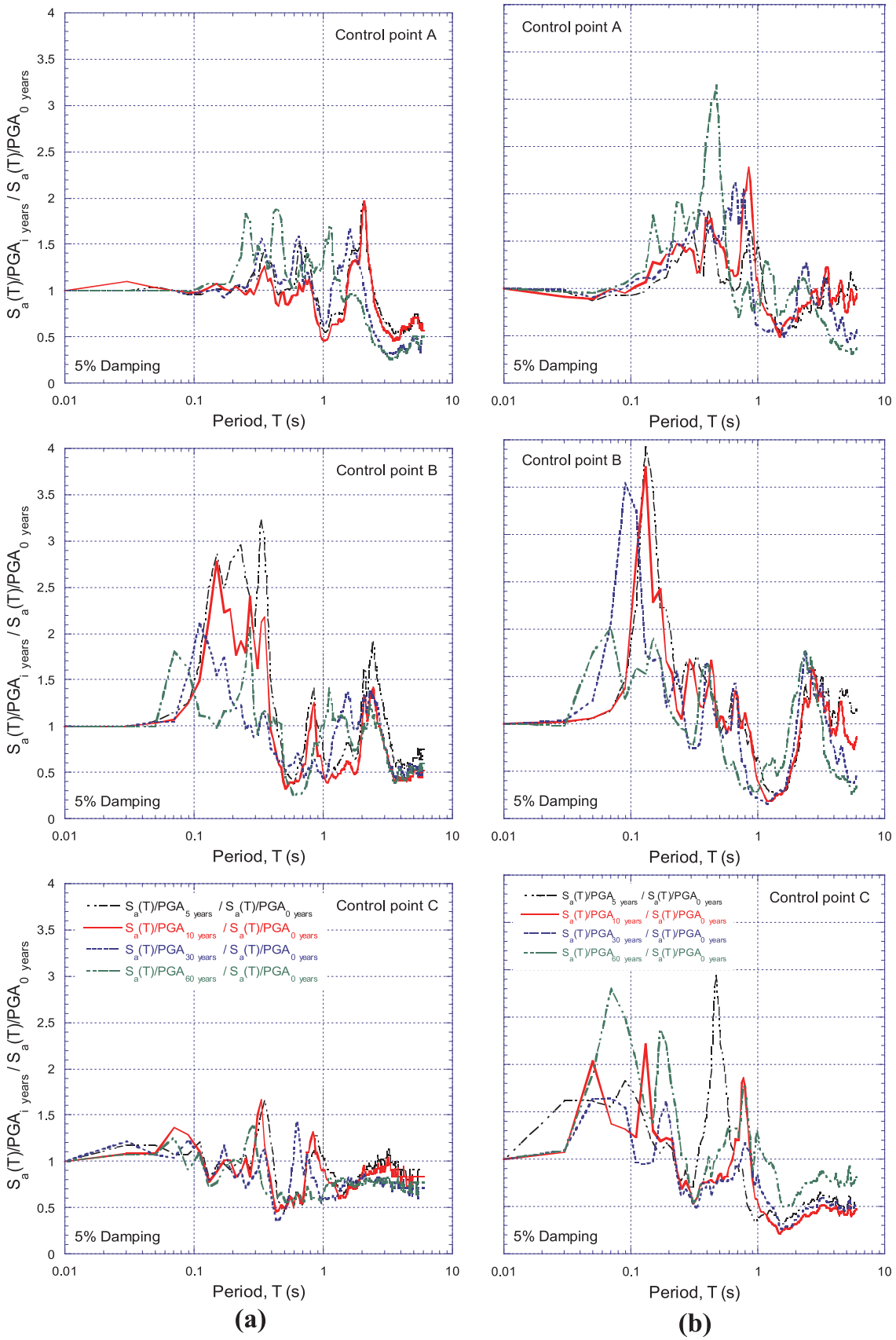

Fig. 27. Normalized evolution of the response spectra with time in control point A, B and C a) Site 1, b) Site 2.

Table 10
Fundamental periods for SSSI in Site 1.

Time	Point A		Point B		Point C	
[years]	T (s)	A[a]	T (s)	A[a]	T (s)	A[a]
0	0.68	3.40	0.60	4.00	0.38	3.80
5	1.25	4.63	0.82	4.10	0.32	2.91
10	1.45	4.68	0.88	3.03	0.33	2.75
30	1.22	4.07	0.70	3.04	0.44	3.14
60	1.32	5.28	0.65	3.10	0.37	2.85

[a] A is amplification ratio S_a/PGA.

Table 11
Fundamental periods for SSSI in Site 2.

Time	Point A		Point B		Point C	
[years]	T (s)	A[a]	T (s)	A[a]	T (s)	A[a]
0	0.46	3.25	0.46	2.90	0.49	3.70
5	0.50	3.77	0.66	4.10	0.53	2.97
10	0.70	4.79	0.85	3.85	0.58	2.15
30	0.83	4.65	1.07	3.62	0.90	3.07
60	1.08	4.85	0.83	2.38	1.07	4.51

[a] A is amplification ratio S_a/PGA.

A similar trend can be observed for Site 2. Nonlinear effects elongates the period at which the maximum spectral response is presented for consolidations times of 5 and 10 years, but after 30 years, the effect of the reduction of layers thicknesses and increase in shear wave velocity, decreases the elastic predominant period, attenuating, in turn, the spectral ordinates. After 60 years of consolidation the elastic fundamental period gets down to 1.09 s, and closer to the lower period at which the energy of the excitation is concentrated, and also to T_{sr}, leading to a large amplification of the soil-structure system response.

7. Conclusions

Soil effective stresses changes during the economic life of a structure built in highly compressible clays leads to important ground deformations, and changes in the dynamic properties (i.e. shear wave velocity distribution and modulus degradation and damping curves). These effects, which are often ignored in practice, can substantially modify the frequency content and spectral accelerations in both free field and in the soil-structure system. Pore pressure variations over the project economic life is due to both regional subsidence as well as dissipation of excess pore pressure caused by the structure weight. For the cases studied herein, a complex interplay between soil nonlinearities, which tend to elongate the fundamental period of the soil deposit, T_p, and the overall tendency of ground consolidation to shorten it, led to variations in the spectral ordinates depending on how close T_p is of the predominant period of the excitation, T_{pe}. For subduction events recorded at Mexico City firm soils T_{pe} ranges between 0.8 and 1.8 s. A similar trend was observed in the soil-structure system response for the cases analyzed inhere. Based on the analyses presented herein, the effect of the changes in dynamic soil properties, and layering configuration should be taken into account in high compressible clays, subjected to rapid regional consolidation rates (i.e. average consolidation rates larger than 10 cm/year), or where the expected primary consolidation settlements over the economic life of the structure exceeds 2.5 m. The key issue is the compressibility of the Mexico City clay, rather than the plasticity. For clays with lower plasticity, or sensitive, but a similar high compressibility, it will be necessary to account for changes in dynamic properties as well as layering configuration, considering that volumetric strain changes in the soil will be associated to changes in the mean consolidation effective stresses. The effect of the lower plasticity will increase the amount of soil nonlinearities developed in the soil and, thus, the amount of pore pressure generated during the cyclic loading. As previously mentioned, this pore pressure will dissipate afterwards, leading to post earthquake-induced settlements. This phenomenon has been studied by several researches, and will eventually also led to soil layer distortion as well as an increase of the dynamic soil properties. Since the effect on the response of a specific soil deposit is also a function of the input motion frequency content, the coupled influence soil properties-input motion characteristics should be evaluated for each condition. Needless to say, this should be taken into account during the design process.

Acknowledgements

Authors would like to thank Grupo Aeroportuario de la Ciudad de México, for sharing some of the laboratory and field results gathered during the design of the New Mexico City Airport. In particular, authors also thanks, Dr. Osvaldo Flores and Zaira Hernández, from the Institute of Engineering at UNAM, which conducted some of the field work and laboratory testing included herein, under the direction of Dr. Ovando Shelley, as well as personnel from Mexican Federal Electricity Commission, CFE. ARUP and TASANA consulting companies also worked on the site characterization in the area, hired by Grupo Aeroportuario de la Ciudad de México, and although these information was not used directly, it also helped as framework for the studies included in this paper. All these information was greatly appreciated.

References

[1] Santoyo E, Ovando E. Underexcavation at the Tower of Pisa and at Mexico´s City Metropolitan Cathedral. Volume Prepared by ISSMGE Technical Committee 36. México: Sociedad Mexicana de Mecánica de Suelos; 2006.
[2] Ovando-Shelley E, Ossa A, Romo MP. The sinking of Mexico City: its effects on soil properties and seismic response. Soil Dyn Earthq Eng 2007;27:333–43.
[3] Ovando-Shelley E, Ossa A, Romo MP. The sinking of Mexico City: its effects on soil properties and seismic response. Soil Dyn Earthq Eng 2007(27):333–43.
[4] Avilés J, Pérez-Rocha LE. Regional subsidence of Mexico City and its effects on seismic response. Soil Dyn Earthq Eng 2010(30):981–9.
[5] Arroyo D, Ordaz M, Ovando-Shelley E, Guasch JC, Lermo J, Perez C, Alcantara L, Ramírez-Centeno MS. Evaluation of the change in dominant periods in the lake-bed zone of Mexico City produced by ground subsidence through the use of site amplification factors. Soil Dyn Earthq Eng 2013;44:54–66.
[6] Schnabel PB, Lysmer J, Seed HB. SHAKE: A Computer Program for Earthquake Responser Analysis of Horizontally Layered Sites. CA: College of Engineering, Report No. EERC 72-12, University of Berkeley; 1972.
[7] Santoyo E History and News of the Regional Sinking of Mexico City. (In Spanish).
[8] The Metropolitan Cathedral. Sinking and rescue. Institute of Engineering at UNAM. First edition. (In Spanish); 2013.
[9] Romo MP, Jaime A, Reséndiz D. General soil conditions and clay properties in the Valley of Mexico. J Earthq Spectra 1988;4(2):731–52.
[10] Seed HB, Romo MP, Sun J, Jaime A, Lysmer J. Relationships between soil conditions and earthquake ground motions. J Earthq Spectra 1988;4(2):687–730.
[11] Mayoral JM, Romo MP, Osorio L. Seismic parameters characterization at Texcoco lake, Mexico. Soil Dyn Earthq Eng 2008;28:507–21.
[12] Mayoral JM, Castañon E, Sarmiento N. Seismic response of high plasticity clays during extreme events. Soil Dyn Earthq Eng 2015;77:203–7.
[13] Flores-Guzmán M, Ovando-Shelley E, Valle-Molina C. Small-strain dynamic characterization of clayey soil from the Texcoco Lake, Mexico. Soil Dyn Earthq Eng 2014;63:1–7.
[14] González CY, Romo MP. Estimation of clay dynamic properties. Rev Ing Sísmica 2011;84:1–23.
[15] Romo MP, Dynamic behavior of Mexico City Clay and its impact in foundation engineering after five years of the earthquake; 1990. p. 125-143 [In Spanish].
[16] Mayne PW, Kulhawy FH. K0-OCR relationships in soil. J Geot Eng Div, ASCE 1982;108(GT6):851–72.
[17] Osorio L, Mayoral JM. Seismic microzonation for the northeast Texcoco lake area, Mexico. Soil Dyn Earthq Eng 2013;48(7):252–66.
[18] Nishenko SP, Singh SK. Conditional probabilities for the recurrence of large and great interplate earthquakes along the Mexican subduction zone. Bull Seismol Soc Am 1987;77(6):2095–114.
[19] Ordaz M, Reyes C. Earthquake hazard in Mexico City: observations versus computations. Bull Seismol Soc Am 1999;89. [1379–83.4].
[20] Zuñiga R, Guzman M. Main seismogenic source zones in Mexico, Technical Report, Seismic Hazard Project, IPGH; 1994.
[21] Rosenblueth E, Ordaz M. Use of seismic data from similar regions. Earthq Eng Struct Dyn 1987;15:619–34.
[22] Arboleda J, Ordaz M. Un mayor uso de los datos estadísticos para estimación de la

sismicidad local/A major use of statistical data for estimation of local seismicity. México: Memoria el X Congreso de Ingeniería Sísmica, Puerto Vallarta Jalisco; 1993. p. 21–7.
[23] Reyes C. State limit of service in building seismic design [Ph.D. thesis]. School of Engineering, National Autonomous University of Mexico (UNAM); 1999.
[24] Singh SK, Rodriguez M, Esteva L. Statistics of small earthquakes and frequency of occurrence of large earthquakes along the Mexican subduction zone. Bull Seismol Soc Am 1983;73:1779–96.
[25] Joyner WB, Boore DM. Peak horizontal acceleration and velocity from strong-motion records including records from the 1979 Imperial Valley, California, earthquake. Bull Seismol Soc Am 1981;71(6):2011–38.
[26] Esteva L. Criteria for the construction of spectra for seismic design, Proceedings of the 3rd Pan-American symposium of structures (Caracas, Venezuela); 3–8 July 1967.
[27] Allin Cornell C. Engineering seismic risk analysis. Bull Seismol Soc Am 1968;58(5):1583–606.
[28] Lilhanand Ky Tseng WS. Development and application of realistic earthquake time histories compatible with multiple damping response spectra. In: Proceedings of the 9th world conference on earthquake engineering (Tokyo, Japan), Vol. II; 1988. p 819–824.
[29] Abrahamson NA. State of the practice of seismic hazard evaluation. Proceedings of GeoEng 2000, Melbourne, 19–24 November, 1; 2000. p. 659–685.
[30] Itasca Consulting Group. FLAC3D, Fast Lagrangian Analysis of Continua in 3 Dimensions, User's Guide (Minneapolis, Minnesota, USA).
[31] Lee C, Tsai Y, Wen K. Analysis if nonlinear site response using the LSST downhole accelerometer array data. Soil Dyn Earthq Eng 2006;26:435–60.
[32] Yee E, Stewart JP, Tokimatsu K. Elastic and large-strain nonlinear seismic site response from analysis of vertical array recordings. J Geotech Geoenviron Eng ASCE 2013;139:1789–801.
[33] Borja RI, Chao H-Y, Montáns FJ, Lin C-H. Nonlinear ground response at lotung lsst site. J Geotech Geoenviron Eng 1999;125(3):187–97.
[34] Borja RI, Chao H-Y, Montáns FJ, Lin C-H. SSI effects on ground motion at lotung LSST site. J Geotech Geoenviron Eng 1999;125(9):760–70.
[35] Borja RI, Wu W-H, Smith HA. Nonlinear response of vertically oscillating rigid foundations. J Geotech Eng 1993;119(5):893–911.
[36] Wang S, Kutter BL, Chacko MJ, Wilson DW, Boulanger RW, Abghari A. Nonlinear seismic soil-pile structure interaction. Earthq Spectra 1998;14(2):377–96.
[37] Paolucci R, Figini R, Petrinia L. Introducing dynamic nonlinear soil-foundation-structure interaction effects in displacement-based seismic design. Earthq Spectra 2013;29(2):475–96.
[38] Borja RI, Amies AP. Multiaxial cyclic plasticity model for clays. J Geotech Eng 1994;120:1051–70.
[39] Ghandil M, Behnamfar F. Ductility demands of MRF structure on soft soils considering soil-structure interaction. Soil Dyn Eart Eng 2017;92:203–14.
[40] Gajan S, Raychowdhury P, Hutchinson TC, Kutter BL, Stewart JP. Application and validation of practical tools for nonlinear soil-foundation interaction analysis. Earthq Spectra 2010;26(1):111–29.
[41] Carlton B, Tokimatsu K. Comparison of equivalent linear and nonlinear site response analysis results and model to estimate maximum shear strain. Earthq Spectra 2016;32(3):1867–87.
[42] Sarmiento N, Martinez A, Romo MP. What is the neutral surface water flow? Is it variable in time? And its consequences. XXVIII National Meeting of Geotechnical Engineering (Merida Yucatan, Mexico). (In Spanish); November 23–26 2016.
[43] Marsal RJy Mazari M. El subsuelo de la ciudad de México/The subsoil of Mexico City, con una revisión de los avances en el conocimiento del subsuelo de la Ciudad de México (1959–2017). Publicado por la UNAM; 2017.
[44] Kuhlemeyer RL, Lysmer J. Finite element method Accuracy for wave propagation problems. J Soil Dyn Div 1973;99:421–7.
[45] Mayoral JM, Argyroudis S, Castañon E. Vulnerability of floating tunnel shafts for increasing earthquake loading. Soil Dyn Earthq Eng 2016;80:1–10.
[46] Mayoral JM, Castañon E, Alcantara L, Tepalcapa S. Seismic response characterization of high plasticity clays. Soil Dyn Earthq Eng 2016;84:174–89.